The Initiation Knot is a Signaling Center Required for Molar Tooth Development

Isabel Mogollón[1], Jacqueline E. Moustakas-Verho[1,2], Minna Niittykoski[1], Laura Ahtiainen[1*]

[1] Cell and Tissue Dynamics Research Program, Institute of Biotechnology, University of Helsinki Finland

[2] Organismal & Evolutionary Biology Research Program, University of Helsinki Finland

Corresponding author L.A.

Cell and Tissue Dynamics Research Program, Institute of Biotechnology/Helsinki Institute of Life Science, P.O. Box 56 (Viikinkaari 5), FIN-00014 University of Helsinki, Finland.

Tel: +358 50 4489338

Email: laura.ahtiainen@helsinki.fi

Summary

Signaling centers, or organizers, regulate many aspects of embryonic morphogenesis. In the mammalian molar tooth, reiterative signaling in specialized centers called enamel knots (EKs) determine tooth patterning. Preceding the first, primary EK, a transient epithelial thickening appears whose significance remains debated. Here, using tissue confocal fluorescence imaging with laser ablation experiments, we show that this transient thickening is an earlier signaling center, the molar initiation knot (IK) that is required for the progression of tooth development. IK cell dynamics manifest the hallmarks of a signaling center; cell cycle exit, condensation, and eventual silencing through apoptosis. IK initiation and maturation are defined by the juxtaposition of high Wnt activity cells to *Shh*-expressing non-proliferating cells, the combination of which drives the growth of the tooth bud, leading to the formation of the primary EK as an independent cell cluster. Overall, the whole development of the tooth, from initiation to patterning, is driven by the iterative use of signaling centers.

Keywords: cell division, migration, embryonic development, tooth, signaling center, Wnt, Shh

Introduction

In recent years, advances in 3D and live tissue imaging have brought new understanding of the cell level behaviors that contribute to the highly dynamic stages of morphogenesis in ectodermal organs, such as hair and teeth (Kim, et al., 2017; Ahtiainen, et al., 2016; Ahtiainen, et al., 2014; Devenport and Fuchs, 2008). Despite shared morphological characteristics and conserved signaling (Biggs and Mikkola, 2014; Jernvall and Thesleff, 2000), it is becoming evident that signaling cues are interpreted into diverse cellular behaviors depending on the context, thereby defining different organ shapes and sizes already at early stages of organogenesis. Morphogenesis in ectodermal organs is regulated by epithelial signaling centers that form sequentially in specific spatiotemporal patterns and govern cell behaviors via secreted factors including hedgehog (Hh), Wnt, fibroblast growth factor (Fgf) and bone morphogenic protein (Bmp) family members (Jernvall and Thesleff, 2000; Dassule and McMahon, 1998).

Teeth have long served as a model organ to study mechanisms of embryonic development in tissue interactions and genetic regulation (Jernvall and Thesleff, 2000). Mice have two tooth types: large ever-growing incisors and multicuspid molars. Organogenesis in teeth is initiated at embryonic day (E)11 with an epithelial thickening called the dental lamina. It resolves into separate domains for incisor and first molar primordia, with a toothless diastema in between. The instructive potential resides initially in the epithelium and shifts to the mesenchyme at the bud stage. Epithelial budding starts at E12.5 followed by mesenchymal condensation leading to a mature bud at E13.5 (Jernvall and Thesleff, 2000). The molar primary enamel knot (pEK) signaling center appears at E13.5 in the late bud stage epithelium and matures into the enamel organ in the cap stage at E14.5 (Tummers and Thesleff, 2009). The pEK is silenced by apoptosis and sequentially followed by pairs of secondary enamel knots (sEK) that regulate cusp patterning (Jernvall, et al., 1994). Fate mapping studies have shown that the pEK clonally contributes to the buccal sEK, but may not contribute to the lingual counterpart (Du, et al., 2017).

The cellular events in early molar morphogenesis have remained largely uncharted, as emphasis has been on the bud stage and beyond. Recently, we identified a novel epithelial signaling center in the early developing incisor, called the initiation knot (IK), which drives local cell proliferation for epithelial budding (Ahtiainen, et al., 2016). The incisor IK shares transcriptional signatures with the incisor enamel knot (EK), which forms without clonal contribution from the IK (Du, et al., 2017; Ahtiainen, et al., 2016; Li, et al., 2016a). While the molar placode and EKs are known to share molecular markers, a similar signaling center in the molar as in the incisor has not been reported. However, previous studies using expression and histological analyses of molar morphogenesis prior to budding, have interpreted a transient epithelial thickening in the diastema anterior to the first developing molar as evidence for the presence of vestigial premolar teeth lost during murine evolution (Prochazka, et al., 2010).

To resolve the early events of molar morphogenesis, we use confocal fluorescence whole-mount live tissue imaging to elucidate the cellular and molecular dynamics of signaling centers and how they shape the tooth bud. We show that an IK signaling center is established in the molar placode and it remains an integral functional part of the developing bud. The molar IK arises by the juxtaposition of cells with high canonical Wnt activity to *Shh*-expressing G_1/G_0-phase cells. Molar early growth is dependent on the IK signaling center and interference of the function of this signaling center either mechanically, by laser ablation, or with specific modulators of relevant signaling pathways, abrogates bud proliferative growth and progression of tooth development. The IK positions the tooth in the growing mandible and is silenced by apoptosis as the pEK arises independently to drive further growth of the bud. The cellular and molecular dynamics of the IK signaling center control tooth development earlier than previously thought.

Results

A molar initiation knot is established in the placode and early bud in G_1/G_0 cells expressing signaling center markers

Cell cycle exit is an early hallmark of ectodermal placodes (Ahtiainen, et al., 2016; Ahtiainen, et al., 2014). The Fucci fluorescent cell cycle reporter system allows direct real-time follow-up of the progress of the cell cycle in individual cells in the developing tissue: When the cell is in G_1/G_0 phase the nucleus emits red fluorescence and upon transition to $S/G_2/M$ proliferative phase, the cell nucleus emits green fluorescence. We used confocal fluorescence microscopy of whole-mount mandibles of the Fucci cell cycle indicator transgenic mouse to characterize G_1/G_0 cell distribution in the developing molar. Transgenic $Shh^{GFP/+}$ (Harfe, et al., 2004) and $Fgf20^{\beta Gal/+}$ expression were used to identify signaling centers from E11.5-E13.5 and EpCam immunofluorescence staining to visualize the epithelium.

At E11.5, G_1/G_0 phase cells were distributed throughout the dental lamina (Fig.1A). By E12.5 the G_1/G_0 cells were located mesially in the mature placode/early bud. At 13.0, the G_1/G_0 focus remained in the mesio-lingual part of the bud, close to epithelial surface and a new focus of G_1/G_0 cells appeared distally deep in the invaginating bud, in the presumptive pEK area. By E13.5, the early G_1/G_0 focus was lost with only a few cells remaining (Fig.1A). Quantification of G_1/G_0 cells in different stages showed a decrease in the G_1/G_0 cell number in the early focus from E12.5 to E13.5 (Fig.S1A). In parallel, G_1/G_0 cells corresponding to the pEK area emerged. For further functional analyses we verified that the budding morphogenesis and G_1/G_0 cell distribution were similar in *ex vivo* cultured whole mount explants to *in vivo* (Fig.S1B). Numbers of G_1/G_0 cells were also similar *in vivo* and in cultured tissue (Fig.S2C).

The Shh^{GFP} and Fucci G_1/G_0 reporters could not be combined as this often resulted in abnormal development of the craniofacial structures. However, the Shh^{GFP} reporter showed expression in the

same areas as the G_1/G_0 foci throughout morphogenesis (Fig.1B): GFP+ cells were present throughout the placode at E11.5. At E12.5, they were located at the mesio-lingual side of the early bud close to the epithelial surface. By E13.5, GFP signal had disappeared almost completely in the early G_1/G_0 focus and appeared in the presumptive pEK area. DIG *in situ* hybridization with a probe specific for *Shh* in Fucci G_1/G_0 reporter mandibles showed exact colocalization of *Shh* with the Fucci reporter (Fig.S1E). The numbers of Shh^{GFP}+ cells and Fucci G_1/G_0 showed similar distribution in the developing molar (Fig.S1A,D). Immunofluorescence staining for β-galactosidase (βGal), marking signaling centers in $Fgf20^{\beta Gal/+}$;Fucci G_1/G_0 embryos, showed colocalization of the markers from E11.5 in the early G_1/G_0 focus and through early bud stage (E12.5-E13.0) and in the pEK at E13.5 (Fig.1C).

Together these data confirmed the identity of the initial molar placode G_1/G_0 focus and corresponding focus in the mesio-lingual part of the developing molar bud epithelium as a signaling center. This early signaling center appeared prior to the pEK and thus we call this signaling center a molar initiation knot (IK).

The molar IK is a functional signaling center driving the molar bud proliferative growth

Next, we studied cell proliferation in the developing molar. In the incisor, budding occurs via cell proliferation regulated by non-proliferative signaling centers (Ahtiainen, et al., 2016), whereas cell rearrangements and migration together with Shh driven proliferation have been proposed as mechanisms for molar bud invagination (Li, et al., 2016b; Prochazka, et al., 2015; Dassule and McMahon, 1998). To dissect the IK contribution to the molar bud, we first studied cell proliferation with Fucci $S/G_2/M$ and G_1/G_0 cell cycle indicators in fixed whole-mount mandibles. We then imaged whole-mount mandible explant cultures using live tissue confocal microscopy, which allowed us to follow the developing bud in a single-cell resolution.

Live tissue confocal microscopy of the Fucci G_1/G_0 reporter, for visualization of the molar IK and pEK cells, and K17-GFP reporter to follow the shape of the epithelial bud from E12.5+16h, confirmed that the IK cells stay an integral part of the developing bud (Fig.2A, Fig.S2A). Observing proliferation patterns with the Fucci reporters showed that during early initiation, at E11.5, G_1/G_0 cells comprised the placode and $S/G_2/M$ cells were evenly distributed throughout the oral epithelium (Fig.2B,C). By E12.5, $S/G_2/M$ cells appeared posterior to the IK in the maturing placode. From E12.5 to E12.75, there was a sharp increase in $S/G_2/M$ cells throughout the bud epithelium, in both basal and suprabasal populations (Fig.2B,C). At E13.5, $S/G_2/M$ cells were present in the bud and surrounding the pEK area. Few IK G_1/G_0 cells still remained. Quantification of cell number showed very few proliferative cells in the placode at E11.5 (Fig.S2B). At E12.5, during the initiation of budding, there was a threefold increase in $S/G_2/M$ cell number and further a twofold increase at E13.0 with similar cell numbers in *ex vivo* cultures (Fig.S2B). Proliferation was concurrent with bud elongation and invagination (Fig.S2C).

We next analyzed the contribution of individual cells in each cell population to the growing bud. Quantification of cell cycle phases with live imaging from E11.5+12h molars showed constant G_1/G_0 cell number in the placode (Fig.2D). A burst of cell proliferation from 4h onwards was seen in the emerging bud. This was specific to the tooth bud, as the contributions of G_1/G_0 and $S/G_2/M$ cells remained constant in the oral epithelium (Fig.2D, Fig.S2D). When we followed individual IK cells through the cell cycle from E11.5+12h, we observed some new G_1/G_0 cells appearing in the IK while two cells showed nuclear fragmentation (Fig.S2E, Mov.S1). None of the followed G_1/G_0 cells in the IK re-entered the cell cycle. Live imaging from the early bud stage onwards E12.0+12h, showed that more bud cells entered $S/G_2/M$ (Fig.S2F, Mov.S2). There was a respective increase in cell divisions throughout the bud as the bud grew. When we followed individual proliferating cells, of the 126 original $S/G_2/M$ cells followed, 25% went through cytokinesis, and divisions were observed throughout the bud (Fig.S2F, Mov.S2). Some IK cells showed nuclear fragmentation and were lost,

while remaining IK cells stayed in G_1/G_0. Quantification of cell cycle phases from E12.5+12h showed that number of molar IK G_1/G_0 cells decreased slightly (Fig.2E). The bud $S/G_2/M$ population continued to expand, leveling out after six hours. This coincided with the appearance of the first G_1/G_0 cells contributing to the pEK. Also, at this stage, proliferation was specific to the tooth bud (Fig.S2D).

Shh and Fgf signaling have been suggested to induce proliferation in tooth buds (Hardcastle et al., 1998, Cobourne et al., 2009); however, inhibition of Shh signaling at the placode stage was reported to produce a flat wide molar bud with negligible effect on proliferation (Prochazka et al., 2015, Li et al., 2016b). This discrepancy could be explained by different effects of the signaling pathway on different molar cell populations. To substantiate this, we treated E11.5 cultures with cyclopamine to inhibit Shh signaling. Inhibition reduced bud invagination (Fig.S3A,C). This was concomitant with a reduced number of proliferating cells with expansion of G_1/G_0 phases adjacent to the IK. A few proliferating cells were still observed basally/peripherally (Fig.S3A,D). We next treated E11.5 cultures with an FGFR inhibitor (SU5402) to examine the role of FGF signaling. Inhibition of FGF signaling induced cell cycle exit somewhat later especially in basal cells, and less reduction in invagination and proliferation compared to cyclopamine treatment (Fig.S3B-D).

We, therefore, conclude that the molar IK is a functional signaling center that regulates proliferation in tooth bud invagination and growth. The molar bud is formed by localized cell proliferation, with the involvement of Shh and FGF signaling.

IK ablation arrests progression of tooth development

To confirm that the IK drives molar bud growth and is necessary for progression of tooth development, we ablated the IK at different developmental stages by microsurgery and laser ablation. When the placode was microsurgically removed at E11.5 and the tissue cultured for 24h, no G_1/G_0 condensate was observed in the diastema and the epithelium remained flat (Fig.S4A,C).

Microsurgical removal of the IK at E12.5 similarly arrested tooth growth, while development on the untreated side proceeded to bud stage with the emerging pEK present (Fig.S4B,C).

For a more targeted approach we next removed the IK G_1/G_0 cells at E11.5, E12.5 and E12.75 with laser ablation, followed by 24h culture, in K17-GFP and Fucci whole mount mandibles. Laser ablation of the IK G_1/G_0 cells in the early placode stage (E11.5) epithelium abrogated epithelial invagination and tooth development, while development in the control progressed normally (Fig.3A,C). Ablation at early bud stage E12.5 similarly completely arrested bud invagination and elongation and inhibited progression of tooth development (Fig.3B,C). Ablation somewhat later at E12.75 at a more developed bud stage also arrested growth; however, a small cluster of G_1/G_0 cells was observed in the bottom of bud facing the mesenchyme in the area where the pEK would emerge (Fig.3D). To observe if the arrested growth resulted from abrogated proliferation, we laser ablated the IK in the Fucci model. Correspondingly, ablation at E11.5 arrested invagination (Fig.3E) and this was accompanied with a loss in cell proliferation in the bud (Fig.3E,F). The persistence of $S/G_2/M$ cells in the adjacent oral epithelium confirmed good tissue health in non-ablated tissue (Fig.3E). Cell proliferation and consequently bud growth were similarly abrogated in E12.5 ablated molars (Fig.3G,H).

These experiments demonstrate that the molar IK is a functional signaling center that drives cell proliferation, thereby regulating tooth bud growth. The IK is, therefore, necessary for the progression of tooth development.

The IK remains an integral part of the developing molar and does not contribute cells to the pEK

We next used whole-mount live tissue imaging to track individual cell movement in the different cell populations in placode and bud stage to dissect whether dynamical cell rearrangements contribute to molar bud formation. Signaling centers show canonical Wnt activity and we used the TCF/Lef:H2B-

GFP reporter to visualize Wnt active cells together with the Fucci G_1/G_0 reporter to track signaling center cells. We further imaged the Fucci G_1/G_0 reporter with the $S/G_2/M$ reporter to follow the proliferating bud cell population.

Initially at E11.5, G_1/G_0 cells were distributed throughout the molar placode (Fig.4A,B,Mov.S3), similarly as observed in fixed samples (Fig.1A). More cells differentiated, entered G_1/G_0 cell cycle phase, and were redistributed mesio-lingually in the maturing placode. Tracking of IK cells showed that they moved toward the mesial front area of the bud remaining an integral part of the bud. In contrast, bud $S/G_2/M$ cells stayed mostly in place (Fig.4B). At E11.5 Wnt activity was seen throughout the dental lamina visualized by high TCF/Lef:H2B-GFP reporter fluorescence intensity (Wnt^{Hi}) (Fig.4C,Mov.S4). The molar placode IK G_1/G_0 cells specifically localized to the peripheral border formed by dental lamina Wnt^{Hi} cells. Some overlap of G_1/G_0 and Wnt^{Hi} signal was seen but the G_1/G_0 cells mostly remained as a distinct subgroup (Fig.4C,D, Mov.S4). More G1 cells were recruited to the IK and they showed directional movement toward the dental lamina Wnt^{Hi} cells. The dental lamina Wnt^{Hi} cells and bud TCF/Lef:H2B-GFP+ cells remained non-motile (Fig.4C,D,Mov.S4).

Tracing cell movement in the molar IK and the emerging pEK from E12.5+12h showed that IK cells remained mesio-lingually close to the bud surface (Fig.4E,F,Mov.S5,Mov.S6). We did not detect contribution from either IK G_1/G_0 cells or Wnt^{Hi} to the pEK (Fig.4G,H,Mov.S6). The pEK arose deep in the bud, without clonal contribution from the IK (Fig.4G,H,Mov.S6). Also at this stage the S/G2/M cells showed little movement with no obvious orientation (Fig.4E,F,Mov.S5) and contribution of cells from oral epithelium, participating in bud growth, was not detected.

Cell condensation and active directional cell migration drive molar IK maturation

Our live imaging experiments showed that IK cells reorganize dynamically during placode/bud maturation. To define the significance of this to IK maturation we quantified IK cell condensation and analyzed if the movements involve active cell migration.

We first measured cell density in EpCam stained fixed whole-mount samples. Initially, at E11.5, G_1/G_0 cells were more dispersed and at E12.5, they had condensed and retained this density until E13.5 (Fig.5A,B). Oral epithelial cells did not show a similar condensation. Quantification of cell density showed that condensation was specific to IK cells, with a significant increase in density from E11.5 to E12.5 compared to the oral epithelium (Fig.5B).

To study if IK condensation is achieved through active cell migration, we followed the movement of individual cells by live imaging at E11.5/E12.5+12h. Tracking showed active migration of the molar IK G_1/G_0 cells at both time points. We quantified the overall track length and net displacement in the different cell populations, and at E11.5+12h, a significant difference in IK G_1/G_0 cells was observed: They migrated more compared to both oral epithelial G_1/G_0 and tooth bud $S/G_2/M$ cells (Fig.5C). At E12.5+12 h, IK G_1/G_0 cells still showed a longer mean track length in the bud compared to S/G2/M cells (Fig.5C). Quantification of IK G_1/G_0 cell displacement angles at E11.5+12h showed a distinct orientation towards the mesio-lingual side of the forming placode/bud, whereas oral epithelial cells showed a random orientation (Fig.5D). We confirmed active migration by following pairs of IK G_1/G_0 and bud $S/G_2/M$ cells that were initially in close proximity (distance$\leq$15µm). The pairwise comparison revealed that while many IK G_1/G_0 cells remained neighbors, 30% of cells switched their partners; most $S/G_2/M$ pairs remained neighbors (Fig.5E). Tracing groups of cells that were initially, at E11.5, located next to each other in different areas of the IK, and defining cell positions 12h later showed that some cells remained close to their original neighbors but several cells ended up with a different group. (Fig.5F). Pharmacological inhibition of acto-myosin based motility, with the inhibitor blebbistatin, repressed IK G_1/G_0 condensation and abrogated progression of tooth development (Fig.5G).

Dynamics between Wnt^{HI} and *Shh* cell populations regulate the maturation and maintenance of the IK

Our live imaging analysis suggested that TCF/Lef:H2B-GFP reporter expressing Wnt^{Hi} cells were closely juxtaposed to *Shh* expressing G_1/G_0 IK cells but they seemed to comprise two different cell populations that remained in close contact with each other through bud development (Fig.6,Mov.S4, Mov.S6,Fig.S1E). The Shh pathway is an important modulator for Wnt signaling for several stages of tooth development. Studies in mouse mutants have implied that Shh is a downstream target of Wnts and also an inhibitor of Wnt signaling via a negative feedback loop (Sarkar, et al., 2000; Sarkar and Sharpe, 1999). We next investigated the behavioral dynamics and the molecular identity of the two populations.

In situ hybridization analysis of Fucci specimens revealed that the IK G_1/G_0 cells colocalized with *Shh* (Fig.S1E). A canonical Wnt, *Wnt10b*, has previously reported expression in the placode (Liu, et al., 2008). When we did a *Wnt10b* hybridization in the Fucci G_1/G_0 reporter, at E11.5; however, *Wnt10b* expression was also detected, partially overlapping, but predominantly anterior to the G_1/G_0 focus (Fig.6D). By E12.5, the dense IK G_1/G_0 colocalized with the *Shh* signal, whereas the *Wnt10b* expression covered a larger area surrounding the IK G_1/G_0 condensate. By E12.75, the diffuse *Wnt10b* expression continued to reside in a wider area in the molar mesio-lingual tip. At E13.0, the G_1/G_0 area was barely discernible and *Shh* and *Wnt10b* were downregulated. Concomitantly, G_1/G_0, *Shh*, and *Wnt10b* expression appeared in the emerging pEK (Fig.S1E, Fig.6A,D). There was a complete spatial correlation with *Shh* and G_1/G_0 signal throughout early molar morphogenesis, but *Wnt10b* expression was seen in the area juxtaposing the G_1/G_0 focus anteriorly.

High resolution analysis of G_1/G_0 and TCF/Lef:H2B-GFP patterns showed that the *Shh*-G_1/G_0 cell population initiated at E11.5 was closely juxtaposed to Wnt^{Hi} cells (Fig.6B,Mov.S4). By E12.5, Wnt^{Hi} cells surrounded the *Shh*-G_1/G_0 cells and TCF/Lef:H2B-GFP+ cells were scarcely distributed in the growing bud prior to pEK appearance (Fig.6B,Mov.S6). At E13.5, Wnt^{Hi} cells were present in the

pEK with G_1/G_0 cells distributed more centrally (Fig.6B). Quantification of *Shh*-G_1/G_0 and Wnt^{Hi} cell populations in fixed samples showed a decrease at E12.5 in *Shh*-G_1/G_0 cell number, concomitant with TCF/Lef:H2B-GFP downregulation and appearance of apoptosis specifically in the IK cells (Fig.6C, Fig.S5A,B) consistent with canonical Wnt signaling activity and *Shh* expression in the maintenance of the IK. To more closely examine this dynamic, we quantified the cell *Shh*-G_1/G_0 and Wnt^{Hi} populations with live imaging in E11.5 and E12.5+12h molars. Quantification at E11.5+12h showed that the number of Wnt^{Hi} cells remained stable for the 12h follow-up; in contrast, the *Shh*-G_1/G_0 cell population increased by 1.5-fold (Fig.6D). Analysis of E12.5+12h cells, showed an increase in Wnt^{Hi} cells, throughout the bud, reaching a plateau after 4h; IK *Shh*-G_1/G_0 cells showed a constant decrease, and G_1/G_0 cells appeared in the pEK from 9h onward (Fig.6D).

Analysis of individual contributing cell populations in the initiation of the molar placode showed a border region with an accumulation of Wnt^{Hi}-*Wnt10b* cells in the dental lamina and the G_1/G_0-*Shh* cells started differentiating closely juxtaposed to this region (Fig.6E). Analysis of cell movement showed differential patterns in the Wnt^{Hi}-*Wnt10b* and G_1/G_0-*Shh* cell populations: track end point analysis showed specific preferential movement of G_1/G_0-*Shh* IK cells toward the dental lamina Wnt^{Hi} cells (Fig.6F) with high straightness (Fig.6G) and high directional persistence in the G_1/G_0-S*hh* IK cell compared to oral epithelial G_1/G_0 and dental lamina Wnt^{Hi} cells (Fig.6H).

The differential distribution and cellular behaviors of Wnt^{Hi} and *Shh*-G_1/G_0 cells in the molar signaling centers suggests that they act in concert to initiate signaling center cell differentiation in the very early stages. The boundary between the two cell populations defines the position of the emerging molar IK and orients the directional migration pattern for condensation. Further, decreased Wnt signaling resulted in *Shh* downregulation and IK clearance.

Modulation of canonical Wnt signaling affects IK cell dynamics and tooth bud shape

The cell movement data suggested the presence of a chemotactic gradient from the dental lamina Wnt^{Hi}-*Wnt10b* cells directing the movement and condensation of the G_1/G_0-*Shh* cell population in molars. *Wnt10b* has been implicated as a paracrine chemotactic factor in epithelial cancer contexts (Chen, et al., 2017; Aprelikova, et al., 2013). To explore if this dynamic occurs in developing molars, we modulated canonical Wnt signaling levels by stimulation with Wnt3a or a Wnt10b releasing bead, and by inhibition with a Wnt antagonist, XAV939 that acts via stimulation of β-catenin degradation and stabilization of axin. E11.5 explants were treated either with Wnt3a/XAV939 in the growth medium for 24h or by placing a recombinant Wnt10b soaked/control bead next to the placode at E11.5 and followed the explants for 16h.

We used K17-GFP to visualize the shape of the epithelium and Fucci G_1/G_0 for IK cell distribution in the developing placode/bud. Stimulation with Wnt3a resulted in a flat bud compared to control (Fig.7A,B), with persisting number of G_1/G_0 IK cells spread out throughout the invagination (Fig.7A,C). Inhibition of active Wnt signaling with XAV939 resulted in a complete loss of G_1/G_0 condensate together with a loss of invagination (Fig.7A). To study if lack of IK condensation and the loss of invagination, with Wnt modulation, was caused by lack of bud cell proliferation, we treated Fucci G_1/G_0; $S/G_2/M$ mandibles with Wnt3a or XAV939. Stimulation with Wnt3a resulted in lack of IK condensation followed by a drastic loss of cell proliferation in the bud (Fig.7D,E). Inhibition with XAV939 resulted in the loss of the G_1/G_0 IK condensate and absence of proliferation and invagination (Fig.7D).

To dissect the role of *Wnt10b* on IK condensation, we placed a Wnt10b releasing or control bead close to the IK distally on the lingual side of the placode and imaged the explants at E11.5, after 8h, and 16h. While morphogenesis and IK condensation proceeded normally in both the control bud and the bud with the control bead, the bud with the Wnt10b bead showed a loss in condensation of the G_1/G_0 IK cells (Fig.7F). Instead, the G_1/G_0 IK cells were spread out toward the Wnt10b bead. Measurement of bud dimensions showed a change in bud shape, e.g. decrease in bud elongation, in

315 Wnt10b bead buds together with a decrease in G_1/G_0 IK cell density (Fig.S6A). The changes in IK

316 cell distribution and bud shape were also accompanied with decrease in proliferation (Fig.S6B, C).

Discussion

The reiterative genetic regulation of tooth development via signaling centers is conserved across tooth types, but it is less understood how it is interpreted into different cellular behaviors to regulate tooth shape and size. In the present study we have identified a molar IK signaling center that is necessary for the progression of tooth development in the early stages of mammalian tooth morphogenesis: We show with live imaging, 4D whole-mount analyses, and functional ablation studies that the IK arises in the placode and is a functional signaling center that drives proliferative growth prior to the successive enamel knots. Molar IK cell dynamics displays the hallmarks of ectodermal signaling centers: cell cycle exit and condensation, and silencing through apoptosis. Cell cycle exit coupled to active condensation, takes place not only in teeth (current study, Ahtiainen et al. 2016), but also in hair placodes (Ahtiainen, et al., 2014). Condensation of the IK via active cell movement is necessary for progression of tooth budding, as inhibition of actomyosin contractility and modulation of condensation guiding Wnt signaling levels, compromised condensation and the function of the signaling center. Cell condensation could be a universal mechanism to both trigger the ectodermal signaling center differentiation and cell cycle exit by contact inhibition of cell proliferation and eventually regulate timing of signaling center silencing by initiating mechanical crowding induced apoptosis.

Tissue recombination studies have shown that the instructive potential in the tooth first resides in the epithelium and shifts only later to the mesenchyme (Lumsden, 1988; Mina and Kollar, 1987). EKs require inductive signals from the mesenchyme, but it is plausible that the IK inducing signal comes from planar epithelial signaling. Wnts*7b/3* and Shh have a mutually exclusive expression already at E10.5 in the presumptive oral and dental ectoderm (Sarkar, et al., 2000; Sarkar and Sharpe, 1999) so it appears that different Wnt expression patterns and *Shh* determine the ectodermal boundaries of competence at a very early stage. *Shh* is possibly a downstream target of Wnts and also a negative feedback inhibitor. Spatial inhibition of *Wnt10b* by *Shh* has been reported in teeth: Shh coated beads

repressed *Wnt10b* but no other epithelial markers (Dassule and McMahon, 1998). Constitutive activation of epithelial Wnt/β-catenin, somewhat later from E12.5, induced multiple patches of signaling center markers, including *Shh* and *Wnt10b* at E13-E14, and ectopic teeth (Liu, et al., 2008; Jarvinen, et al., 2006). Our work evidences that *Wnt10b* and *Shh* are differentially expressed during molar initiation and that these cell populations remain functionally separate. However, close interaction between the G_1/G_0-*Shh* and Wnt^{Hi}-*Wnt10b* expressing cells is crucial in the positioning and maintenance of the molar IK. Wnt10b has been implicated as a paracrine chemotactic factor in cancer contexts (Chen, et al., 2017; Aprelikova, et al., 2013). The migration of G_1/G_0-*Shh* IK cells toward the canonical Wnt gradient and specific area of endogenous *Wnt10b* expression and distribution of IK cells toward exogenous source of recombinant Wnt10b, suggest that *Wnt10b* carries an instructive role in signaling center condensation.

We show that molar invagination and growth take place through cell proliferation in both basal and suprabasal bud cell populations, driven by the non-proliferative IK. Several signaling pathways regulate behaviors in these cell populations, but the role of Hh signaling in this context has been debated. Shh has been interpreted to be a primary inducer of proliferation in some experimental settings, whereas other studies suggest a role in bud cell rearrangement (Li, et al., 2016b; Prochazka, et al., 2015; Cobourne, et al., 2009; Hardcastle, et al., 1998). *Shh* expression is a hallmark of signaling centers, and while autocrine signaling cannot be ruled out, most of the responsive cells seem to reside elsewhere: at later stages, from E14.5 onwards, the pEK expresses *Shh* but receptor *Ptch* and downstream targets *Gli1/2/3* are expressed in the mesenchyme (Hardcastle, et al., 1998; Vaahtokari, et al., 1996a). In early stages from E11.0, the transducer *Smo* is ubiquitously expressed, whereas *Ptch1* and *Gli1* are mostly in the mesenchyme (Dassule and McMahon, 1998; Hardcastle, et al., 1998). Interestingly, by E12.0, the expression of both *Ptch1* and *Gli1/2* have been reported in the emerging epithelial bud. Notably, in our analyses, proliferation coincided with this. The inhibition of Shh signaling at the placode stage resulted in loss of proliferation in the bud. Thus, it seems that in

the IK, *Shh* expressing cells are different from Shh responsive cells and signaling can induce proliferation. In agreement, early findings from conditional *Shh* mutants show smaller teeth and posteriorly misplaced buds (Dassule, et al., 2000; Dassule and McMahon, 1998). In the limb bud, Shh has been reported to affect proliferation both directly and indirectly via induction of Fgfs in the AER (Prykhozhij and Neumann, 2008; Towers, et al., 2008). In the tooth, other factors downstream of the initial placodal inducer Shh, such as Fgfs, likely contribute to bud invagination via proliferation mainly in basal cells, and possibly concurrent with stratification (current study, (Li, et al., 2016b).

Expression levels of *Shh* may specifically affect signaling center identity, differentiation, and maintenance. *Shh* overexpression arrests development at the bud stage due to lack of proliferation, and multiple superficial invaginations are induced in the epithelium but still fail to develop further (Cobourne, et al., 2009). It is tempting to hypothesize that exogenous *Shh* expression would drive cells into abnormal cell cycle exit and/or a change in fate into a signaling center. Signaling center maintenance may also be associated with *Shh* expression levels. Shh has been shown to be protective of early apoptosis in the tooth (Cobourne, et al., 2001). Apoptosis is a mechanism used to silence signaling centers in teeth, the AER of the limb, and in embryonic brain development (Nonomura, et al., 2013; Matalova, et al., 2004; Vaahtokari, et al., 1996b). The interplay between Wnt^{Hi} and *Shh*+ cells may serve as a feedback mechanism regulating the timing of apoptosis in the IK.

We demonstrate that the pEK in the molar is formed de novo without clonal contribution from the IK, and that the IK is apoptotically silenced upon pEK appearance. This differs mechanistically from signaling centers later in molar development, where the pEK contributes cells to sEKs (Du, et al., 2017). The development of teeth is conserved, however, in being driven by the iterative use of signaling centers. We have shown functionally here that the progression of early molar morphogenesis is dependent on the IK signaling center that arises in the placode and exhibits many hallmarks of ectodermal signaling centers. What differentiates the IK from the later signaling centers on a transcriptomic level will be of special interest to future studies.

Acknowledgments

We thank Frederic Michon and Jukka Jernvall for critical reading of the manuscript. Imaging was done at the Light Microscopy Unit/Institute of Biotechnology, University of Helsinki. The work was financially supported by the Academy of Finland, the Sigrid Jusélius Foundation, Finnish Cultural Foundation and Helsinki Institute of Life Sciences.

The authors declare no competing financial interests.

Author Contributions

Conceptualization L.A. and I.M.; Methodology, I.M., M.N., L.A.; Investigation I.M., M.N., L.A; Writing Original draft, L.A., I.M. and J.M-V; Writing, Review and Editing L.A., I.M., J.M-V and M.N.; Funding Acquisition L.A.; Supervision L.A.

403 ## References

404 Ahtiainen, L., Lefebvre, S., Lindfors, P.H., Renvoise, E., Shirokova, V., Vartiainen, M.K., Thesleff,
405 I., and Mikkola, M.L. (2014). Directional cell migration, but not proliferation, drives hair placode
406 morphogenesis. Developmental cell 28, 588-602.
407 Ahtiainen, L., Uski, I., Thesleff, I., and Mikkola, M.L. (2016). Early epithelial signaling center
408 governs tooth budding morphogenesis. J Cell Biol 214, 753-67.
409 Aprelikova, O., Palla, J., Hibler, B., Yu, X., Greer, Y.E., Yi, M., Stephens, R., Maxwell, G.L.,
410 Jazaeri, A., Risinger, J.I., et al. (2013). Silencing of miR-148a in cancer-associated fibroblasts
411 results in WNT10B-mediated stimulation of tumor cell motility. Oncogene 32, 3246-53.
412 Biggs, L.C., and Mikkola, M.L. (2014). Early inductive events in ectodermal appendage
413 morphogenesis. Seminars in cell & developmental biology 25-26, 11-21.
414 Chen, Y., Zeng, C., Zhan, Y., Wang, H., Jiang, X., and Li, W. (2017). Aberrant low expression of
415 p85alpha in stromal fibroblasts promotes breast cancer cell metastasis through exosome-mediated
416 paracrine Wnt10b. Oncogene 36, 4692-4705.
417 Cobourne, M.T., Hardcastle, Z., and Sharpe, P.T. (2001). Sonic hedgehog regulates epithelial
418 proliferation and cell survival in the developing tooth germ. J Dent Res 80, 1974-9.
419 Cobourne, M.T., Xavier, G.M., Depew, M., Hagan, L., Sealby, J., Webster, Z., and Sharpe, P.T.
420 (2009). Sonic hedgehog signalling inhibits palatogenesis and arrests tooth development in a mouse
421 model of the nevoid basal cell carcinoma syndrome. Dev Biol 331, 38-49.
422 Dassule, H.R., Lewis, P., Bei, M., Maas, R., and McMahon, A.P. (2000). Sonic hedgehog regulates
423 growth and morphogenesis of the tooth. Development 127, 4775-85.
424 Dassule, H.R., and McMahon, A.P. (1998). Analysis of epithelial-mesenchymal interactions in the
425 initial morphogenesis of the mammalian tooth. Dev Biol 202, 215-27.
426 Devenport, D., and Fuchs, E. (2008). Planar polarization in embryonic epidermis orchestrates global
427 asymmetric morphogenesis of hair follicles. Nat Cell Biol 10, 1257-68.

Du, W., Hu, J.K., Du, W., and Klein, O.D. (2017). Lineage tracing of epithelial cells in developing teeth reveals two strategies for building signaling centers. J Biol Chem 292, 15062-15069.

Fliniaux, I., Mikkola, M.L., Lefebvre, S., and Thesleff, I. (2008). Identification of dkk4 as a target of Eda-A1/Edar pathway reveals an unexpected role of ectodysplasin as inhibitor of Wnt signalling in ectodermal placodes. Dev Biol 320, 60-71.

Hardcastle, Z., Mo, R., Hui, C.C., and Sharpe, P.T. (1998). The Shh signalling pathway in tooth development: defects in Gli2 and Gli3 mutants. Development 125, 2803-11.

Harfe, B.D., Scherz, P.J., Nissim, S., Tian, H., McMahon, A.P., and Tabin, C.J. (2004). Evidence for an expansion-based temporal Shh gradient in specifying vertebrate digit identities. Cell 118, 517-28.

Huh, S.H., Jones, J., Warchol, M.E., and Ornitz, D.M. (2012). Differentiation of the lateral compartment of the cochlea requires a temporally restricted FGF20 signal. PLoS Biol 10, e1001231.

Jarvinen, E., Salazar-Ciudad, I., Birchmeier, W., Taketo, M.M., Jernvall, J., and Thesleff, I. (2006). Continuous tooth generation in mouse is induced by activated epithelial Wnt/beta-catenin signaling. Proceedings of the National Academy of Sciences of the United States of America 103, 18627-32.

Jernvall, J., Kettunen, P., Karavanova, I., Martin, L.B., and Thesleff, I. (1994). Evidence for the role of the enamel knot as a control center in mammalian tooth cusp formation: non-dividing cells express growth stimulating Fgf-4 gene. Int J Dev Biol 38, 463-9.

Jernvall, J., and Thesleff, I. (2000). Reiterative signaling and patterning during mammalian tooth morphogenesis. Mechanisms of development 92, 19-29.

Kim, R., Green, J.B.A., and Klein, O.D. (2017). From snapshots to movies: Understanding early tooth development in four dimensions. Dev Dyn 246, 442-450.

Li, C.Y., Hu, J., Lu, H., Lan, J., Du, W., Galicia, N., and Klein, O.D. (2016a). alphaE-catenin inhibits YAP/TAZ activity to regulate signalling centre formation during tooth development. Nat Commun 7, 12133.

Li, J., Chatzeli, L., Panousopoulou, E., Tucker, A.S., and Green, J.B. (2016b). Epithelial stratification and placode invagination are separable functions in early morphogenesis of the molar tooth. Development 143, 670-81.

Liu, F., Chu, E.Y., Watt, B., Zhang, Y., Gallant, N.M., Andl, T., Yang, S.H., Lu, M.M., Piccolo, S., Schmidt-Ullrich, R., et al. (2008). Wnt/beta-catenin signaling directs multiple stages of tooth morphogenesis. Dev Biol 313, 210-24.

Lumsden, A.G. (1988). Spatial organization of the epithelium and the role of neural crest cells in the initiation of the mammalian tooth germ. Development 103 Suppl, 155-69.

Martin, P. (1990). Tissue patterning in the developing mouse limb. Int J Dev Biol 34, 323-36.

Matalova, E., Tucker, A.S., and Sharpe, P.T. (2004). Death in the life of a tooth. J Dent Res 83, 11-6.

Mina, M., and Kollar, E.J. (1987). The induction of odontogenesis in non-dental mesenchyme combined with early murine mandibular arch epithelium. Arch Oral Biol 32, 123-7.

Narhi, K., and Thesleff, I. (2010). Explant culture of embryonic craniofacial tissues: analyzing effects of signaling molecules on gene expression. Methods Mol Biol 666, 253-67.

Nonomura, K., Yamaguchi, Y., Hamachi, M., Koike, M., Uchiyama, Y., Nakazato, K., Mochizuki, A., Sakaue-Sawano, A., Miyawaki, A., Yoshida, H., et al. (2013). Local apoptosis modulates early mammalian brain development through the elimination of morphogen-producing cells. Developmental cell 27, 621-34.

Prochazka, J., Pantalacci, S., Churava, S., Rothova, M., Lambert, A., Lesot, H., Klein, O., Peterka, M., Laudet, V., and Peterkova, R. (2010). Patterning by heritage in mouse molar row development. Proceedings of the National Academy of Sciences of the United States of America 107, 15497-502.

476 Prochazka, J., Prochazkova, M., Du, W., Spoutil, F., Tureckova, J., Hoch, R., Shimogori, T.,
477 Sedlacek, R., Rubenstein, J.L., Wittmann, T., et al. (2015). Migration of Founder Epithelial Cells
478 Drives Proper Molar Tooth Positioning and Morphogenesis. Developmental cell 35, 713-24.
479 Prykhozhij, S.V., and Neumann, C.J. (2008). Distinct roles of Shh and Fgf signaling in regulating
480 cell proliferation during zebrafish pectoral fin development. BMC Dev Biol 8, 91.
481 Sakaue-Sawano, A., Kurokawa, H., Morimura, T., Hanyu, A., Hama, H., Osawa, H., Kashiwagi, S.,
482 Fukami, K., Miyata, T., Miyoshi, H., et al. (2008). Visualizing spatiotemporal dynamics of
483 multicellular cell-cycle progression. Cell 132, 487-98.
484 Sarkar, L., Cobourne, M., Naylor, S., Smalley, M., Dale, T., and Sharpe, P.T. (2000). Wnt/Shh
485 interactions regulate ectodermal boundary formation during mammalian tooth development.
486 Proceedings of the National Academy of Sciences of the United States of America 97, 4520-4.
487 Sarkar, L., and Sharpe, P.T. (1999). Expression of Wnt signalling pathway genes during tooth
488 development. Mechanisms of development 85, 197-200.
489 Shirokova, V., Jussila, M., Hytonen, M.K., Perala, N., Drogemuller, C., Leeb, T., Lohi, H., Sainio,
490 K., Thesleff, I., and Mikkola, M.L. (2013). Expression of Foxi3 is regulated by ectodysplasin in
491 skin appendage placodes. Dev Dyn 242, 593-603.
492 Towers, M., Mahood, R., Yin, Y., and Tickle, C. (2008). Integration of growth and specification in
493 chick wing digit-patterning. Nature 452, 882-6.
494 Tummers, M., and Thesleff, I. (2009). The importance of signal pathway modulation in all aspects
495 of tooth development. J Exp Zool B Mol Dev Evol 312B, 309-19.
496 Vaahtokari, A., Aberg, T., Jernvall, J., Keranen, S., and Thesleff, I. (1996a). The enamel knot as a
497 signaling center in the developing mouse tooth. Mechanisms of development 54, 39-43.
498 Vaahtokari, A., Aberg, T., and Thesleff, I. (1996b). Apoptosis in the developing tooth: association
499 with an embryonic signaling center and suppression by EGF and FGF-4. Development 122, 121-9.

500 Wang, J., and Shackleford, G.M. (1996). Murine Wnt10a and Wnt10b: cloning and expression in

501 developing limbs, face and skin of embryos and in adults. Oncogene 13, 1537-44.

Figure Legends

Figure 1. A molar initiation knot is established in the molar placode and early bud in G_1/G_0 cells positive for signaling center markers

Confocal fluorescence images of mouse embryonic mandibles of the cell cycle indicator (Fucci) for G_1/G_0 phase (red) and signaling center marker Shh^{GFP}(green) and $Fgf20^{\beta Gal}$(βGal staining, magenta) Immunofluorescence staining of the epithelium (EpCam, grey, dotted line), early G_1/G_0 focus (arrowhead), presumptive primary enamel knot (pEK)(asterisk). Planar view from the mesenchyme toward the epithelium. (A) G_1/G_0 phase cells were present throughout the dental lamina and the molar placode, as incisor and molar resolved into separate domains at E11.5. At E12.5, G_1/G_0 cells formed a focus mesially in the molar early bud. This focus remained close to epithelial surface mesio-lingually. At E13.0, G_1/G_0 cells corresponding to the presumptive pEK emerged in the tip of the bud and condensed by E13.5. (B) Shh^{GFP} reporter and (C) $Fgf20^{\beta Gal}$ signaling center marker showed expression corresponding to G_1/G_0 foci throughout placode and bud morphogenesis and in the emerging pEK.

Figure 2. The molar IK is a functional signaling center driving budding via proliferation

(A) Still images of live tissue confocal microscopy of the Fucci G_1/G_0 reporter to visualize the molar IK cells and K17-GFP (green) reporter to visualize the borders and shape of the epithelial bud from E12.5+16h showed that the IK stays an integral part of the developing bud. (B) Confocal fluorescence images of whole mount explants Fucci G_1/G_0 (red), $S/G_2/M$ (green), epithelium (EpCam, white, dotted line), IK (arrowhead) and pEK (asterisk). Initially $S/G_2/M$ cells were seen throughout the oral epithelium and by E12.5, in the early bud posterior to the IK in both basal and suprabasal populations. IK and pEK cells remained in G_1/G_0 phase. (C) Surface rendering of the nuclei in G_1/G_0 and $S/G_2/M$ cell cycle phases in the developing molar placode/bud epithelium. (D) Quantification of cell cycle phases in live imaging E11.5+12h and (E) E12.5+12h molars (N=5, N=3, mean±SEM).

Figure 3. Laser ablation of the IK arrests molar bud growth

Confocal fluorescence images of whole mount explant cultures K17-GFP/ Fucci S/G_2/M (green), Fucci G_1/G_0 (red), tooth placode/bud epithelium (dotted line), Hoechst (blue), IK (arrowhead) and pEK (asterisk). The IK was laser ablated (position marked with a viewfinder symbol ¤) at E11.5, E12.5 or E12.75 followed by 24h culturing. (A) Laser ablation of the IK G_1/G_0 cells in the early placode stage (E11.5) epithelium abrogated epithelial invagination and growth. In the control tooth invagination proceeded normally. (B) Early bud stage (E12.5) ablation completely arrested bud invagination and elongation. (C) Bud dimensions of ablated and control molars at E11.5+24h and E12.5+24h (fold change over E11.5, $N_{E11.5+24h}$=9, $N_{E12.5+24h}$=8, mean±SEM, Mann-Whitney U,* $p \leq 0.05$, ** $p \leq 0.01$, *** $p \leq 0.001$). (D) Ablation at E12.75 arrested bud growth. However, a cluster of G_1/G_0 cells emerged in the bottom of bud in the epithelium mesenchyme interface. (E) Laser ablation of the IK in the Fucci S/G_2/M model at E11.5 resulted in loss of bud cell proliferation. S/G_2/M cells present in the adjacent oral epithelium confirmed good tissue health. (F) Quantification of proliferating cells in E11.5+24h molars (N=8, mean±SEM Mann-Whitney U, $p \leq 0.001$). (G) Bud cell proliferation and consequently bud growth were similarly abrogated in E12.5 ablated molars. (H) Quantification of proliferating cells in E12.5+24h molars (fold change over E12.5, N=8, mean±SEM Mann-Whitney U, $p \leq 0.01$).

Figure 4. The IK remains an integral part of the tooth and does not contribute cells to the pEK that arises independently

(A) Still images of a Fucci G_1/G_0 (red) and $S/G_2/M$ (green) live tissue time lapse confocal imaging from placode stage E11.5+12h. (B) Tracks and displacement vectors of individual cells at E11.5+12h molar Fucci G_1/G_0, $S/G_2/M$, placode epithelium border (dotted line). (C) Still images of a Fucci G_1/G_0 (red) and TCF/Lef:H2B-GFP (green) reporter time lapse E11.5+12h. (D) E11.5+12h cell tracks and displacement of individual Fucci G_1/G_0, TCF/Lef:H2B-GFP, cells and cells positive for both reporters. (E) Still images of a Fucci G_1/G_0 and $S/G_2/M$ reporter live imaging form early bud stage E12.5+12h. (F) E12.5+12h cell tracks and displacement of individual Fucci G_1/G_0 and $S/G_2/M$ cells (G) Still images of a Fucci G_1/G_0 and TCF/Lef:H2B-GFP live imaging E12.5+12h. (H) Cell tracks and displacement E12.5+12h Fucci G_1/G_0, TCF/Lef:H2B-GFP, and Fucci G_1/G_0+TCF/Lef:H2B-GFP.

Figure 5. Cell condensation and active directional cell migration drive molar IK maturation

(A) Confocal fluorescence images of Fucci G_1/G_0 (red) molars, cell borders (EpCam, white, dotted line), Hoechst (blue). (B) Quantification of IK and oral epithelial cell density ($N_{placode/bud}=N_{oral}=10$, Mann-Whitney U, $p\leq0.001$). (C) Quantification cell of track length and net displacement in molar placode/bud and oral epithelium at E11.5+12h ($N_{G1/G0\ IK}=149$, $N_{G1/G0\ oral}=45$, $N_{S/G2/M}=146$, Mann-Whitney U, $p\leq0.001$***) and E12.5+12 h ($N_{G1/G0\ IK}=90$, $N_{G1/G0\ oral}=51$, $N_{S/G2/M}=317$, Mann-Whitney U, $p\leq0.05$). (D) Quantification of molar IK and oral epithelial cell movement angles E11.5+12h. ($N_{IK\ cells}=N_{oral\ epithelial\ cells}=95$, Rayleigh test: H_0=random, IK $p\leq0.001$, oral $p>0.05$). (E) Pairwise comparison of molar IK G_1/G_0 and bud S/G_2M cell positions ($N_{pairs}=40$, Mann-Whitney U test, *$p\leq0.05$)*. (F) Tracing of groups of cells at E11.5 that resided close to each other (respectively color coded) and positions of the individual cells 12h later. Cells switching neighbors (asterisk). (G) Confocal fluorescence whole mount images of Fucci G_1/G_0 (red) and K17-GFP (green) reporter. E11.75 cultures were treated at the time of most active IK G_1/G_0 cell movement with blebbistatin for 24h to inhibit actomyosin based cell motility. Blebbistatin treatment repressed IK G_1/G_0 cell condensation and arrested bud morphogenesis.

Figure 6. Dynamics between Wnt^{HI} and *Shh* cell populations regulate the maturation and maintenance of the IK

(A) Fucci G_1/G_0 fluorescence images overlaid with whole-mount DIG *in situ* hybridization for *Wnt10b*. (B) Single cell resolution analysis of Fucci G_1/G_0 (red) and TCF/Lef:H2B-GFP (green), reporter for active Wnt/β-catenin signaling, patterns. EpCam (white, dotted line), IK (arrowhead) and pEK (asterisk). At E11.5, TCF/Lef:H2B-GFP high intensity (Wnt^{Hi}) was present in the dental lamina and the molar IK G_1/G_0 condensate was located next to a border of Wnt^{Hi} cells. At E12.5, IK G_1/G_0 only cells were surrounded by Wnt^{Hi} cells. At E13.5, G_1/G_0 and Wnt^{Hi} cells were present in the presumptive pEK region. (C) Quantification number of cells in Wnt^{Hi}, G_1/G_0 and double positive cell populations in fixed samples ($N_{E11.5}$=413; $N_{E12.5}$=192; E13.5 N_{IK}=136 N_{pEK}=831, mean±SEM, non-parametric Student's t-test, $p\leq0.05$*, $p\leq0.01$**, $p\leq0.001$***). (D) Quantification of cell number in each population from live tissue imaging E11.5+12h and E12.5+12h ($N_{E11.5+12h}$ =$N_{E12.5+12h}$=3, mean±SEM). (E) Surface rendering still images of E11.5+12h molar time-lapse, Fucci G_1/G_0, TCF/Lef:H2B-GFP, and double cells. At E11.5+3h onwards the G_1/G_0 cell population started differentiating closely juxtaposed to Wnt^{Hi} cells with increasing number of cells transitioning to G_1/G_0. (F) Track end point analysis (median: red cross, $N_{IK\ G1/G0}$=128, $N_{oral\ G1/G0}$=63, N_{WntHi}=104). Molar IK G_1/G_0 cells showed preferential distribution toward the Wnt^{Hi} region (forward). (G) Track straightness in molar IK G_1/G_0, oral epithelial G_1/G_0 and TCF/Lef:H2B-GFP+ cell populations ($N_{IK\ G1/G0}$=128, $N_{oral\ G1/G0}$=42, N_{WntHi} =67, Mann-Whitney U, $p\leq0.001$). (E) Decay of cellular persistence ($N_{IK\ G1/G0}$=80, $N_{oral\ G1/G0}$=50, N_{WntHi}=71).

Figure 7. Modulation of canonical Wnt signaling affects IK cell dynamics and molar bud shape

(A) Confocal fluorescence images of explants cultures K17-GFP (green), Fucci G_1/G_0 (red), tooth placode/bud epithelium (dotted line). Canonical Wnt signaling levels were modulated from placode stage E11.5+24h by stimulation with Wnt3a, of inhibition with XAV939. Stimulation resulted in a flat bud with persisting G_1/G_0 IK cells throughout the invagination. Inhibition lead to a complete loss of the G_1/G_0 condensate and abrogated invagination. (B) Quantification of bud dimensions in Wnt3a stimulated and control cultures (fold change over E11.5, $N_{ctrl}=12$, $N_{Wnt3a}=10$, mean±SEM, Mann-Whitney U, $p\leq0.001$). (C) Quantification of IK cell number, density and area in Wnt3a stimulated and control cultures (fold change over E11.5, $N_{ctrl}=12$, $N_{Wnt3a}=10$, mean±SEM, Mann-Whitney U, $p\leq0.001$). (D) Stimulation with Wnt3a in Fucci G_1/G_0; $S/G_2/M$ cultures resulted in lack of IK condensation followed by a drastic loss of cell proliferation in the bud. Inhibition with XAV939 resulted in the loss of the G_1/G_0 IK condensate and absence of proliferation and invagination (E) Quantification of cell proliferation in Wnt3a stimulated and control cultures (fold change over E11.5, $N_{ctrl}=7$, $N_{Wnt3a}=8$, mean±SEM, Mann-Whitney U, $p\leq0.01$). (F) A Wnt10b recombinant protein releasing or control bead was placed close to the IK (visualized with Fucci G_1/G_0 reporter) distally on the lingual side of the placode and the explants were imaged at E11.5, after 8h, and 16h. Morphogenesis and IK condensation proceeded normally in control buds without beads and with a control bead. The Wnt10b bead showed a loss in condensation of the G_1/G_0 IK cells. Instead the G_1/G_0 IK cells were spread out toward the Wnt10b bead.

612 ## Materials and Methods

613 ### Animals, tissues preparation and culture treatments

614 All mouse studies were approved by the National Animal Experiment Board. Transgenic mouse
615 reporter lines: fluorescent cell cycle indicator (Fucci) mice express a nuclear red fluorescent reporter
616 in G_1/G_0 phase (Cdt1-mKO) and green fluorescent reporter in $S/G_2/M$ phases (Gem-mAZ) (Sakaue-
617 Sawano, et al., 2008). Shh^{GFPCre} mice (#005622, Jackson Laboratories) express GFP consistent with
618 endogenous *Shh* locus marking signaling centers (Harfe, et al., 2004), K17-GFP mice visualize the
619 tooth epithelium (#023965, Jackson Laboratories). TCF/Lef:H2B-GFP mice, are indicators of Wnt/β-
620 catenin signaling, containing several copies of TCF/Lef1 DNA binding sites driving expression of
621 the H2B-EGFP fusion protein (#013752; Jackson Laboratories); $FGF20^{\beta Gal}$ mice have an Fgf20-β-
622 galactosidase (βGal) knock-in allele (Huh, et al., 2012). Embryos were staged according to limb
623 morphological criteria; vaginal plug day was embryonic day (E)0.5 (Martin, 1990).

624 Embryonic mandibles were dissected at E11.5-E13.5 and whole mount explants where fixed from 2h
625 to overnight in 4% PFA or cultured in a Trowell-type tissue culture as described previously (Narhi
626 and Thesleff, 2010). For live imaging experiments tissues where maintained in D-MEM/F12 without
627 phenol red and supplemented with 50U/ml penicillin, 50µg/ml streptomycin, 10% FCS and HEPES
628 15mM (Gibco). For inhibitor/activator treatments samples were dissected at E11.5 or E11.75, and
629 vehicle or smoothened inhibitor cyclopamine was applied for inhibition of Shh signaling (50µM;
630 Sigma-Aldrich), blebbistatin to inhibit actomyosin mediated cell motility (100µM; Sigma-Aldrich),
631 pan-FGFR inhibitor SU5420 (20µM; Calbiochem), recombinant Wnt3a (10ng/ml; R&D Systems) for
632 stimulation and XAV939 (10µM; Tocris) to inhibit canonical Wnt signaling was added to the growth
633 medium for 24h. For bead implantation, heparin acrylic beads (MCLAB) were incubated with
634 100µg/ml recombinant human Wnt10b protein (0.1mg/ml;R&D Systems) at 37°C for 30 minutes.
635 Control beads were soaked with similar concentrations of BSA under the same conditions. Protein-

636 soaked beads were stored at 4°C and used within one week. Beads were applied on tissue explant
637 cultures at E11.5 distally on the lingual side of the placode and tissues were imaged at the start point,
638 after 8 and 16h to ensure good tissue condition.

639 **Whole mount immunofluorescence, fluorescence microscopy and *in situ***
640 **hybridization**

641 For whole mount immunofluorescence staining fixed tissues were permeabilized with 0.5% TritonX-
642 100 for 2h RT and washed with PBS. Unspecific staining was blocked by incubation in 5% normal
643 donkey/goat serum, 0.3% BSA, 0.1% TritonX-100 in PBS 1h RT. Tissues were incubated overnight
644 in +4°C with the primary antibody rat polyclonal anti-mouse CD326 (EpCam, 1:1000, Pharmingen),
645 rabbit polyclonal βGal (1:400, MP Biomedicals), rabbit polyclonal cleaved caspase 3 (1:400, Cell
646 Signaling Technologies) or goat polyclonal sonic hedgehog antibody (1:100, R&D Systems) and
647 detected with Alexa Fluor-488, Alexa Fluor-568 or Alexa Fluor-647 conjugated secondary antibodies
648 (1:500, BD and Invitrogen) and nuclei were stained with Hoechst 33342. Tissues were mounted with
649 Vectashield (Vector Laboratories) and imaged with either Leica Biosystems TCS SP5 microscope
650 and HC PL APO 10×/0.4 (air), HCX PL APO 20×/0.7 Imm Corr (water, glycerol, oil) Lbd.bl and
651 HCX APO 63×/1.30 Corr (glycerol) CS 21 objectives or Zeiss LSM700 microscope and HC PL APO
652 10×/0.45 (air) and LD LCI PL APO 25×/0.8 Imm Corr (water, glycerol, oil) objectives. For analysis
653 of TCF/Lef:H2B-GFP signal intensities, the cutoff value for high and low expressing cells was
654 adjusted according to overall signal intensity in each sample. All results represent at least three
655 independent experiments.

656 For combined fluorescence and whole mount *in situ* hybridization analyses: Fluorescent imaging for
657 fixed Fucci G_1/G_0 reporter whole mount mandibles was first done with a Zeiss SteREO Lumar.V12
658 microscope, NeoLumar S 0.8×/WD 80-mm objective, and Zeiss Axiocam MRm3 CCD camera. The
659 samples where then subjected to whole mount *in situ* hybridization with digoxigenin-labeled probes
660 specific for *Shh* or *Wnt10b* performed as described previously (Shirokova, et al., 2013; Fliniaux, et

al., 2008; Wang and Shackleford, 1996). Imaging of the hybridization signal was done with the same Zeiss Lumar microscope and Zeiss AxioCam ICc1 CCD camera and images were transposed.

Fluorescence confocal microscopy and time-lapse imaging and laser ablation

For 3D time-lapse imaging dissected tissues were allowed to recover for a minimum of 2h prior to imaging. The explants were imaged as described previously (Ahtiainen, et al., 2016; Ahtiainen, et al., 2014) with an upright Leica Biosystems TCS SP5 microscope, HC PL APO 10×/0.4 (air) objective in a trowel-type culture setup. Z-stacks of 3µm optical sections were acquired at 20min intervals. Good tissue health was confirmed by lack of pyknotic nuclei and frequency of mitoses in every acquired z-stack. For determination of cell cycle status and cell quantification, only cells that were distinctly identified as either G_1/G_0 or $S/G_2/M$ were scored. For Wnt/β-catenin signaling activity TCF/Lef:H2B-GFP cells were scored individually for median fluorescence intensity in each nucleus and presence of G_1/G_0 signal. All results represent at least three independent experiments.

Laser ablations were done with an upright Leica Biosystems TCS SP5 microscope, HC PL APO 10×/0.4 (air) objective and a tunable Ti:Sapphire pulsed IR laser (Spectra Physics, MaiTai, tunable range 690-1040nm) at room temperature with an excitation wavelength 800nm and 2.95W of laser power (100%) for 3-10 seconds. The pulse was targeted to the IK, visualized with the Fucci reporter, using zoom factor 20-40x. Efficiency of ablation was verified by acquiring confocal fluorescence Z-stacks of the sample immediately after ablation. After 24h of culture tissues were fixated, Fucci cell cycle reporter samples were immunofluorescence stained with EpCam to visualize the epithelium, and all samples were stained with Hoechst 33342 to visualize nuclei. Samples were imaged with the Zeiss LSM700 microscope, with HC PL APO 10×/0.45 (air) and LD LCI PL APO 25×/0.8 Imm Corr (glycerol) objectives. Specificity of ablation was verified by the absence of Fucci G_1/G_0 phase (Cdt1-mKO) positive cells in the IK region and ablation of only the epithelial compartment visualized with the K17-GFP reporter and Hoechst staining. Good tissue health of the adjacent, non-ablated tissue,

was confirmed by lack of pyknotic nuclei and presence of normal cell proliferation patterns with the Fucci reporter.

Quantitative and statistical analyses of experimental data

Analyses of images and quantitative measurements were done with Imaris 9.0.1 (Bitplane) and ImageJ software. Images were processed for presentation with Photoshop CC and Illustrator CC software (Adobe Systems). Statistical analysis and further graphing were done with PAST (http://folk.uio.no/ohammer/past/; Hammer et al., 2001), and SPSS Statistics (IBM) software.

Measurements were done from whole mount volume renderings of confocal optical Z-stacks. For quantifying cell density individual cell borders were visualized and traced in 3D with the EpCam staining in whole-mount tissues. Cell densities were quantified by masking a volume in tooth epithelium/equal volume in the oral epithelium, and defined as areas occupied by the cell (selecting a cross section in 3D view in the middle of the cell). Box-and-whiskers plots represent minimum, 25th percentile, median, 75th percentile, and maximum values for each dataset. Differences between groups were assessed with the Mann-Whitney U test.

All cell movement, follow up and division analyses were done from stereoscopic 3D renderings, allowing exact localization of cells in three dimensions, and in time. Individual cell track length and net displacement were measured in signaling center and oral epithelial cells. The distribution of cell trajectory displacement angles was analyzed with the Rayleigh test (H0=random, $p>0.05$). For IK G_1/G_0 group and pairwise cell trajectory analysis tissues were live imaged E11.5+12h. G_1/G_0 cells where divided into neighboring groups in their original position and traced to the end position. Cells within close proximity of each other (≤15µm) were analyzed in pairs. For the analysis on decay of cellular persistence in directional migration, we first determined the angle of cell migration during the first hour of observation for the initial orientation of the cells. At each following time point, cells that had not yet turned > ±90° from their starting angle, were considered directionally persistent.

Supplemental Figure Legends

Related to Figure 1.

Figure S1. Mandible explants grown *in vitro* show same cell behavioral and morphogenetic developmental patterns as in *in vivo*

For functional live tissue imaging analyses we first verified that cultured explants developed, in respect to G_1/G_0 cell population dynamics and bud growth, comparably to *in vivo* development. (A) Quantification of G_1/G_0 cells in the developing molar placode and bud *in vivo* (embryos $N_{E11.5}=7$, $N_{E12.5}=11$, $N_{E13.0}=4$ $N_{E13.5}=5$, error bars±SEM). (B) Confocal fluorescence images of mouse embryonic mandible explants at E12.5 and grown *ex vivo* in a Trowell culture setup for 8h, 22h or 28h. Fucci fluorescent cell cycle indicator G_1/G_0 (Fucci G1)(red), K17-GFP epithelial placode/bud marker and immunofluorescence staining for a pan-epithelial marker EpCam (grey), epithelium (dotted line). Explants show similar morphogenesis to *in vivo* with a slight lag in timing. (C) Quantification of G_1/G_0 cells in the developing molar placode and bud *in vitro* in cultured explants (embryos $N_{E12.5+8h}=2$, $N_{E12.5+24h}=8$, $N_{E12.5+27h}=7$, mean±SEM) (D) Quantification of Shh-GFP cells in the IK and emerging pEK *in vivo* (embryos $N_{E11.5}=4$, $N_{E12.5}=11$, $N_{E13.0}=3$ $N_{E13.5}=5$, error bars±SEM). (E) Fucci G_1/G_0 fluorescence images overlaid with whole-mount DIG *in situ* hybridization with a probe specific for *Shh*. Molar IK G_1/G_0 focus (arrowhead), emerging pEK (asterisk).

Related to Figure 2.

Figure S2. Tooth epithelial cell populations contribute differentially to the growing bud

(A) IK cells remain an integral part of the developing early molar bud. Graph shows the distribution of individual IK G_1/G_0 cells (cell tracks in dark grey) and emerging pEK cells (cell tracks in light grey) to the growing bud imaged from E12.5 up to 16h (image z-stacks taken at 20min intervals). Color scale represents borders of the growing tooth bud visualized with K17-GFP. (B) Quantification of $S/G_2/M$ cell number in developing molars *in vivo* ($N_{E11.5}$=7, $N_{E12.5}$=8, $N_{E13.0}$=4, $N_{E13.5}$=5, mean±SD) was similar to explants grown *ex vivo (*$N_{E12.5+8h}$=4, $N_{E12.5+22h}$=7, $N_{E12.5+28h}$=4, mean±SD). (C) Quantification of molar bud dimensions *in vivo* (black bars) and *ex vivo* cultured explants (white bars) Dimensions in width and length were similar *in vivo* and cultured specimens with somewhat flatter bud after culturing ($N_{E11.5}$=5, $N_{E12.5}$=11, $N_{E13.0}$=4, $N_{E13.5}$=5, $N_{E12.5+8h}$=4, $N_{E12.5+22h}$=10, $N_{E12.5+28h}$=7, mean±SD). (D) Quantification of cell cycle phases in oral epithelial cells of Fucci G_1/G_0 and S/G2/M whole mount live imaging samples from E11.5+12h (N=5, mean±SEM) and E12.5+12h (N=3, mean±SEM). (E) Surface rendering composite still image of a live tissue whole mount time lapse E11.5+12h. Tracing the contribution of individual G_1/G_0 and $S/G_2/M$ cells originating from various positions in the bud, G_1/G_0 (red), $S/G_2/M$ (green) and cell divisions (white numbers). Divisions (where cytokinesis was observed) in surface rendering shown mother and daughter cells respectively color coded. Line graph shows the contribution of individual G_1/G_0 and $S/G_2/M$ cells to the molar from E11.5+12h. (F) Surface rendering composite still image of a live tissue whole mount time lapse E12.0+12h and line graph showing the contribution of individual G_1/G_0 and $S/G_2/M$ cells.

746 **Related to Figure 2.**

747 **Figure S3. Shh is involved in bud proliferation and inhibition of Hh or Fgf signaling**
748 **suppresses invagination**

749 (A) Confocal fluorescence images of Fucci G_1/G_0, $S/G_2/M$ whole mount explants cultured
750 E11.5+24h. Samples were treated with cyclopamine for inhibition of Shh signaling, or vehicle (Ctrl).
751 Fucci G_1/G_0 (red) $S/G_2/M$ (green) and epithelial EpCam immunofluorescence staining (white). At
752 E11.5, at the start of treatment the IK was emerging. After 24h in culture the control showed
753 invagination with $S/G_2/M$ cells in the bud adjacent to the IK distally. Cyclopamine treatment resulted
754 in an expansion of G_1/G_0 phase cells and reduced proliferation adjacent to the IK. (B) Fucci whole
755 mount explants cultured E11.5+24h. Samples were treated with an FGFR inhibitor (SU5420) or
756 vehicle (Ctrl). After 24h of treatment with SU5402, some proliferative cells were present but there
757 was an increase in G_1/G_0 phase cells particularly in the basal population (arrows). (C) Quantification
758 of bud depth (fold change over start of the treatment) in E11.5+24h samples treated with cyclopamine
759 or SU5402 ($N_{cyclo}=6$, $N_{SU5402}=4$, mean±SEM, Mann Whitney U, $p\leq0.01$**, $p\leq0.001$***). (D)
760 Quantification of G_1/G_0 and $S/G_2/M$ cells in the bud (N in all groups=5, mean±SEM, Mann Whitney
761 U, $p\leq0.01$**).

762 **Related to Figure 3.**

763 **Figure S4. Microsurgical removal of the IK abrogates molar bud growth**

764 Confocal fluorescence images of Fucci G_1/G_0 (red) whole mount explant cultures, EpCam
765 immunofluorescence staining (white, epithelium marked with a dotted line), nuclei Hoechst (blue).
766 (A) The molar epithelial placode was microsurgically removed at E11.5 and the tissue cultured for
767 24h. No G_1/G_0 condensate was present in the diastema and the epithelium remained flat while the
768 control bud invaginated normally. (B) Microsurgical removal of the IK at E12.5 similarly arrested
769 molar growth. The control side development proceeded normally to bud stage with the emerging pEK
770 present. (C) Quantification of epithelial bud depth on the control side compared to epithelium depth
771 in the respective area on the side where the IK was microsurgically removed in E11.5+24h and
772 E12.5+24h explants ($N_{E11.5+24h}$=8, $N_{E12.5+24h}$=7, mean±SEM, Mann Whitney U, $p \leq 0.05$*, $p \leq 0.01$**)

773 **Related to Figure 6.**

774 **Figure S5. Apoptosis as a silencing mechanism of the molar IK signaling center**

775 (A) Whole mount confocal fluorescence images of Fucci G_1/G_0 (red), cleaved caspase 3
776 immunofluorescence staining for apoptotic cells (Casp3, green). Epithelial bud (dotted line), IK
777 (arrowhead) and presumptive pEK (asterisk), volume rendering from side view of molar. (B)
778 Quantification of Casp3+ nuclei in the molar IK (N=12, mean±SEM).

779 **Related to Figure 7.**

780 **Figure S6. Apoptosis as a silencing mechanism of the molar IK signaling center**

781 (A) Quantification of bud length and IK G_1/G_0 cell density (fold change over start of the treatment)
782 in E11.5+16h samples with a recombinant Wnt10b protein releasing or control bead close to the IK
783 distally on the lingual side of the placode compared to control (N=10, mean±SEM, Mann Whitney
784 U, $p \leq 0.05$*). (B) Confocal fluorescence images of Fucci G_1/G_0 (red), $S/G_2/M$ (green) whole mount
785 explant cultures, EpCam immunofluorescence staining (white, epithelium marked with a dotted line),
786 bead (closed circle). (C) Quantification of $S/G_2/M$ cells at E11.5+16h (fold change over start of the
787 treatment) in Wnt10b bead treated molar buds compared to untreated control buds (N=6, mean±SEM,
788 Mann Whitney U, $p \leq 0.05$*).

789 **Supplemental Movie Legends**

790 **Related to Figure 2.**

791 **Movie S1. Tracking individual cell G1 and S/G2/M fates in a Fucci cell cycle reporter E11.5+12h**
792 **molar placode by live tissue confocal imaging shows placode IK cells stay in G1 phase**

793 Fluorescence confocal microscopy time-lapse of an embryonic mouse E11.5 whole-mount mandible
794 explant imaged for 12h. Image stacks were taken at 20min intervals, and the playback speed here is
795 five frames per second. The tracking of individual cell fates from the placode stage is shown as a
796 surface rendering of the Fucci cell cycle indicator: the contribution of individual G_1/G_0 phase cells in
797 the placode and initiation knot are shown color coded in red hues and $S/G_2/M$ cells in green.
798 Individual cell divisions of mother cells and their daughters are color coded in blue, green and yellow
799 shades, respectively. IK G_1/G_0 cells in the placode did not re-enter the cell cycle. In contrast
800 neighboring cells, distally from the IK, frequently entered $S/G_2/M$ phase and cell divisions
801 contributed to invagination locally.

802 **Related to Figure 2.**

803 **Movie S2. The IK remains an integral part of the growing tooth bud as shown in Fucci cell**
804 **cycle reporter E12.0+12 h molars by confocal live tissue imaging**

805 Fluorescence confocal microscopy time-lapse of a Fucci cell cycle indicator E12.0 whole-mount
806 mandible explant imaged for 12h. Image stacks were taken at 20min intervals, and the playback speed
807 here is five frames per second. The tracking of individual cell fates during the early bud invagination,
808 is shown as a surface rendering: G_1/G_0 phase cells are shown in red hues and S/G2/M cells in green.
809 Individual cell divisions of mother cells and their daughters are color coded in blue, green and yellow
810 shades, respectively. IK cells remained in G_1/G_0 phase and remained an integral part of the growing
811 tooth. $S/G_2/M$ phase cells and cell divisions in both basal and suprabasal populations contributed to
812 invagination and growth throughout the bud.

Related to Figure 4.

Movie S3. Live imaging of Fucci cell cycle reporter shows that IK cells rearrange dynamically in the E11.5+12h molar placode

Fluorescence confocal microscopy time-lapse of an embryonic mouse E11.5 whole-mount mandible explant imaged for 12h, showing the contribution of cell cycle stages to molar placode and initial budding morphogenesis on a high single cell resolution. Image stacks were taken at 20min intervals, and the playback speed here is five frames per second. The movie shows a volume rendering of cell cycle indicator Fucci G_1/G_0 nuclei (red) and $S/G_2/M$ (green). First, an overview of the mandible at the start of imaging seen from the mesenchymal side toward the epithelium, then a close up of the developing molar placode (IK, open circle) followed by both channels merged and separately. Individual cell tracks are shown as a dragon tail rendering showing a subset of twenty subsequent points in each track, IK G_1/G_0 (red), $S/G_2/M$ (green). The IK G_1/G_0 cells moved toward the mesial front area of the bud. The IK cells stayed in G_1/G_0 phase and drove proliferation locally in the adjacent cells, posterior to the knot, to initiate the invagination of the epithelium. The bud $S/G_2/M$ cells showed little movement.

828 **Related to Figures 3, 4 and 6.**

829 **Movie S4. Live imaging shows TCF/Lef:H2B-GFP and Fucci G1 marker expressing cells are**
830 **closely juxtaposed and exhibit differential movement patterns in E11.5+12h molar placodes**

831 Fluorescence confocal microscopy time-lapse of E11.5+12h Fucci G_1/G_0 and TCF/Lef:H2B-GFP
832 reporters. Image stacks were taken at 20min intervals, and the playback speed here is five frames per
833 second. The movie shows a volume rendering of Fucci G_1/G_0 nuclei (red) and TCF/Lef:H2B-GFP
834 canonical Wnt signaling reporter (green). First an overview of the mandible at the start of imaging
835 seen from the mesenchymal side toward the epithelium, then a close up of the developing molar
836 placode (IK, open circle) followed by both channels merged and separately. Individual cell tracks are
837 shown as a dragon tail rendering showing a subset of ten subsequent points in each track, IK G_1/G_0
838 (red), TCF/Lef:H2B-GFP (green), both reporters (yellow). The molar placode IK G_1/G_0 cells
839 specifically localized to the peripheral border formed by dental lamina cells with high TCF/Lef:H2B-
840 GFP reporter expression (Wnt^{Hi} cells). Increasing numbers of G_1/G_0 cells were recruited to the IK
841 with directional movement, toward the dental lamina Wnt^{Hi} cells. Dental lamina Wnt^{Hi} cells remained
842 mostly localized.

Related to Figures 3 and 4

Movie S5. Live imaging of E12.5+12h Fucci reporter shows that IK G1 cells do not contribute clonally to the primary EK in the molar

Fluorescence confocal microscopy time-lapse of E12.5+12h Fucci explant, showing the contribution of cell cycle stages at bud stage and initiation of the pEK. Image stacks were taken at 20min intervals, and the playback speed here is five frames per second. The movie shows volume rendering of Fucci G_1/G_0 nuclei (red) and $S/G_2/M$ (green) overview of the mandible at the start of imaging (initial molar bud outlined white). In the close up of the molar IK is marked with an open circle and the location where the pEK will be initiated (marked with a closed circle). Time lapse shows volume rendering of both channels merged and separately. In track view the perimeter of the mature bud is outlined in white. Individual cell tracks are shown as a dragon tail rendering showing a subset of ten subsequent points in each track, IK G_1/G_0 (red), pEK G_1/G_0 (magenta), $S/G_2/M$ (green). A wave of cell proliferation contributed to rapid bud growth while the IK cells stayed in G_1/G_0 in the mesial part of the bud. The pEK G_1/G_0 cells were initiated *de novo* deep in the tip of the invaginating bud with no clonal contribution from the IK.

858 **Related to Figures 4.**

859 **Movie S6. Live imaging of Fucci and TCF/Lef:H2B-GFP reporters shows independent IK and**
860 **pEK signaling centers regulating morphogenesis in E12.5+12h molar**

861 Fluorescence confocal microscopy time-lapse of Fucci G_1/G_0 and TCF/Lef:H2B-GFP E12.5+12h
862 whole mount explant. The movie shows volume rendering of Fucci G_1/G_0 nuclei (red) and
863 TCF/Lef:H2B-GFP canonical Wnt signaling reporter (green) visualizing the IK and emerging pEK
864 signaling centers. Image stacks were taken at 20 min intervals, and the playback speed here is five
865 frames per second. An overview of a volume rendering of the mandible at the start of imaging shows
866 both channels merged and the molar bud is outlined in white. In close up view of the molar IK position
867 is marked with an open circle and the location where the pEK is later initiated is marked with a closed
868 circle. Time lapse shows volume rendering of both channels merged and separately. In track view the
869 perimeter of the mature bud is outlined in white. Individual cell tracks are shown as a dragon tail
870 rendering showing a subset of ten subsequent points in each track, IK G_1/G_0 (red), pEK G_1/G_0
871 (magenta), high intensity TCF/Lef:H2B-GFP (Wnt^{Hi}, green), double positive (Wnt^{Hi}+ Fucci G_1/G_0,
872 yellow). Initially at E12.5, Wnt^{Hi} cells surrounded the G1 cells in the IK. TCF/Lef:H2B-GFP positive
873 cells appeared throughout the bud with increase in signal intensity in the prospective pEK region
874 followed by emergence of first G1 cells. Tracking of individual G_1/G_0, Wnt^{Hi}, and double positive
875 cells showed that none of these cell populations from the IK contributed clonally to the pEK; the
876 Wnt^{Hi} and G_1/G_0 cells in the pEK region appeared *de novo*.

Figure 1.

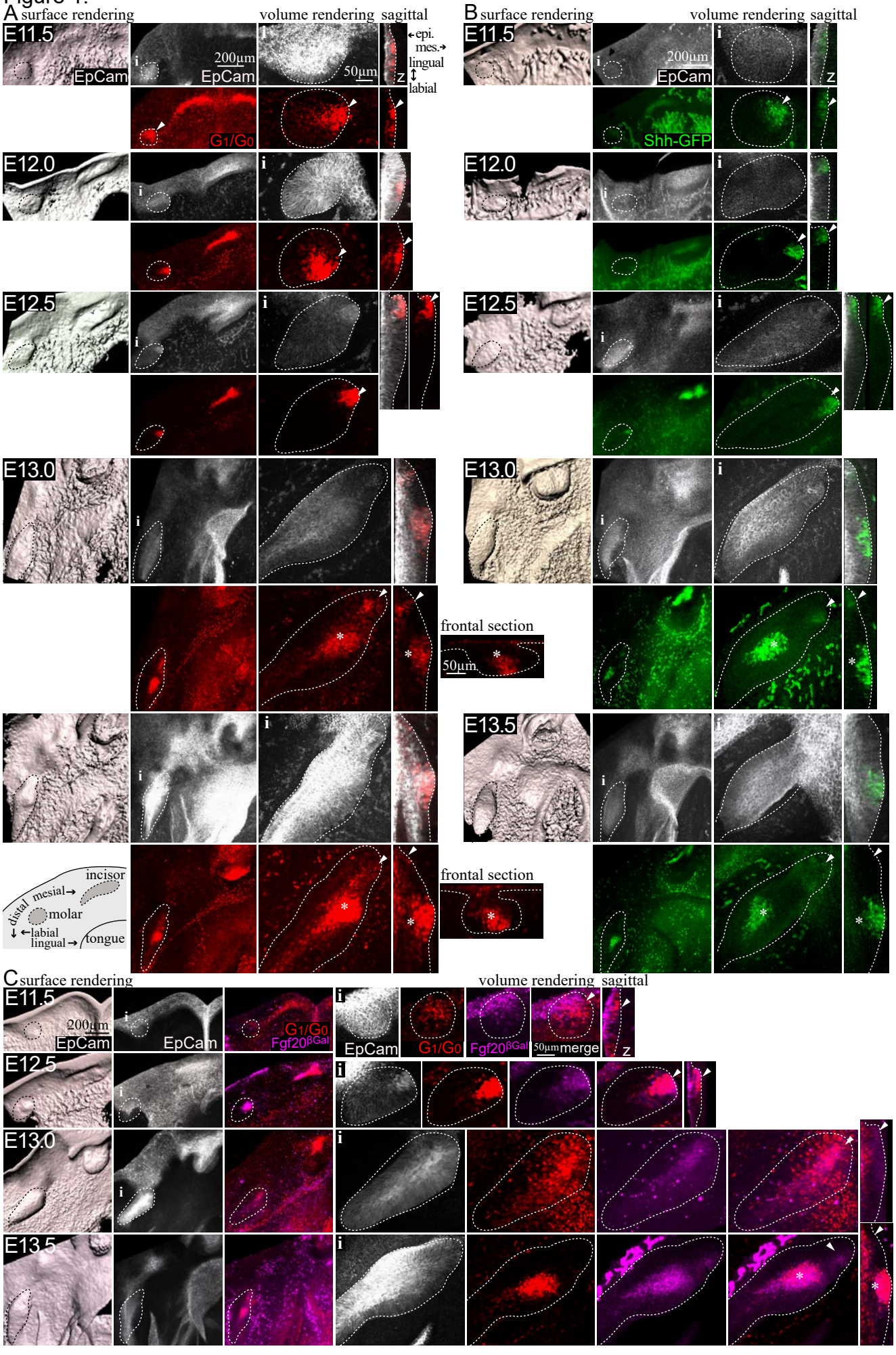
A surface rendering
volume rendering sagittal
B surface rendering
volume rendering sagittal
E11.5
E12.0
E12.5
E13.0
E13.5
EpCam
G1/G0
Shh-GFP
200μm
50μm
epi.
mes.
lingual
labial
frontal section
incisor
mesial
distal
molar
labial
lingual
tongue
C surface rendering
volume rendering sagittal
Fgf20βGal
merge

Figure 2.

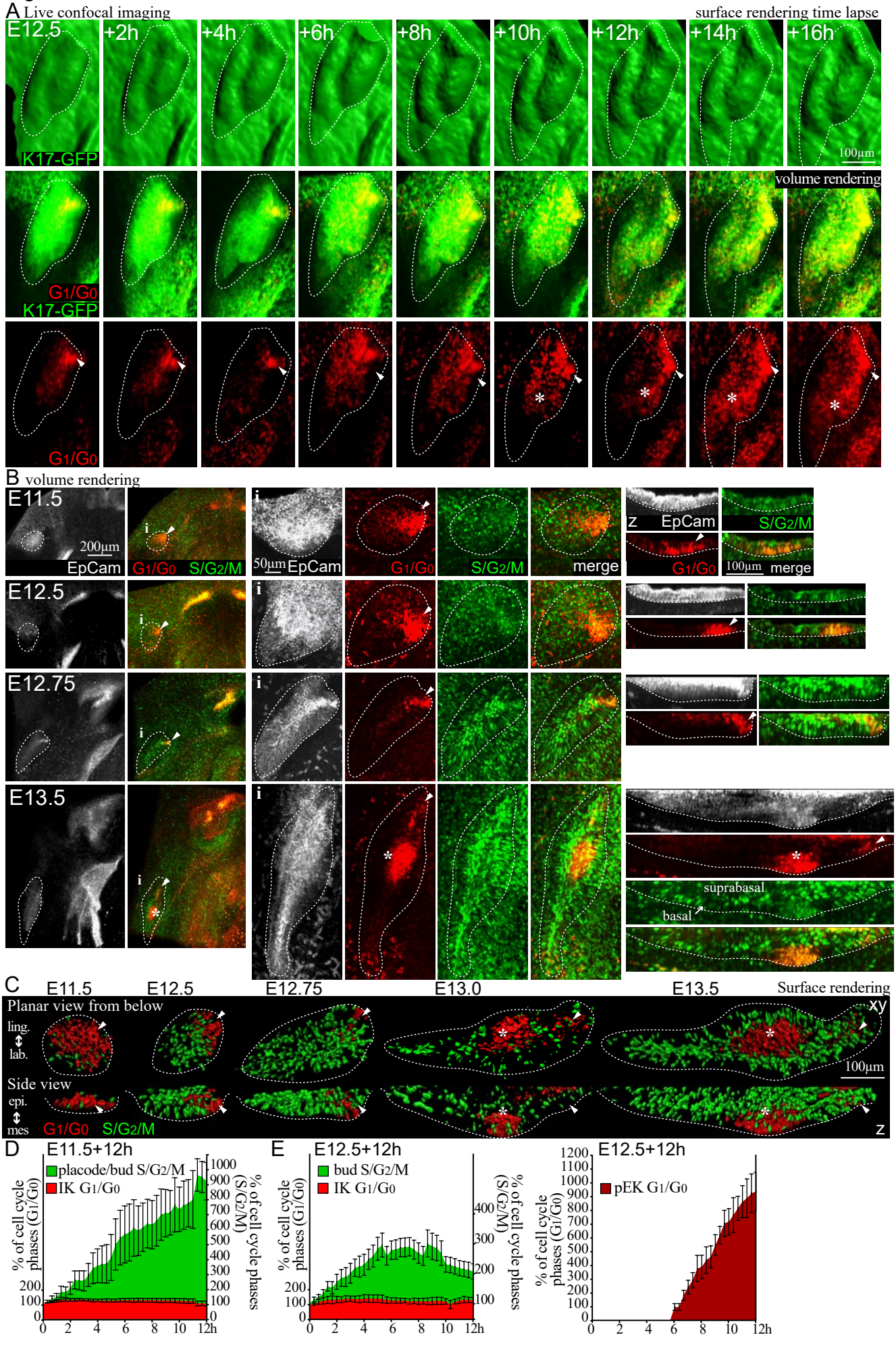
A Live confocal imaging
surface rendering time lapse
E12.5
+2h
+4h
+6h
+8h
+10h
+12h
+14h
+16h
K17-GFP
100µm
volume rendering
G1/G0
K17-GFP
G1/G0
B volume rendering
E11.5
200µm
EpCam
G1/G0
S/G2/M
50µm
EpCam
G1/G0
S/G2/M
merge
z
EpCam
S/G2/M
G1/G0
100µm
merge
E12.5
E12.75
E13.5
suprabasal
basal
C
E11.5
E12.5
E12.75
E13.0
E13.5
Surface rendering
Planar view from below
ling.
lab.
xy
100µm
Side view
epi.
mes
G1/G0
S/G2/M
z
D
E11.5+12h
placode/bud S/G2/M
IK G1/G0
% of cell cycle phases (G1/G0)
% of cell cycle phases (S/G2/M)
E
E12.5+12h
bud S/G2/M
IK G1/G0
% of cell cycle phases (G1/G0)
% of cell cycle phases (S/G2/M)
E12.5+12h
pEK G1/G0
% of cell cycle phases (G1/G0)

Figure 3.

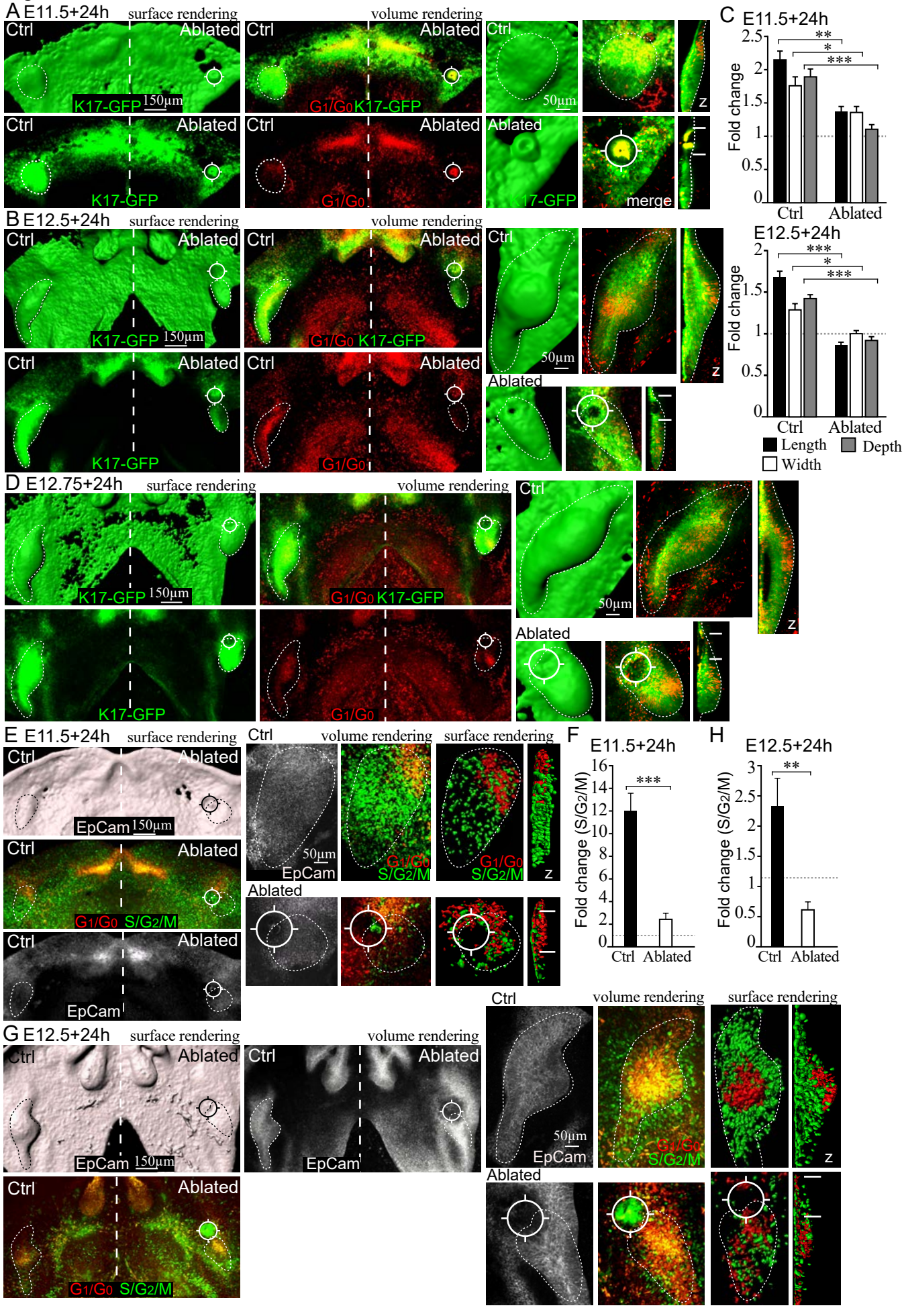
A E11.5+24h
surface rendering
volume rendering
Ctrl
Ablated
K17-GFP
150μm
G1/G0 K17-GFP
G1/G0
50μm
z
17-GFP
merge
B E12.5+24h
C E11.5+24h
E12.5+24h
Fold change
Ctrl
Ablated
Length
Depth
Width
D E12.75+24h
E E11.5+24h
EpCam
G1/G0 S/G2/M
F E11.5+24h
Fold change (S/G2/M)
H E12.5+24h
G E12.5+24h

Figure 4.

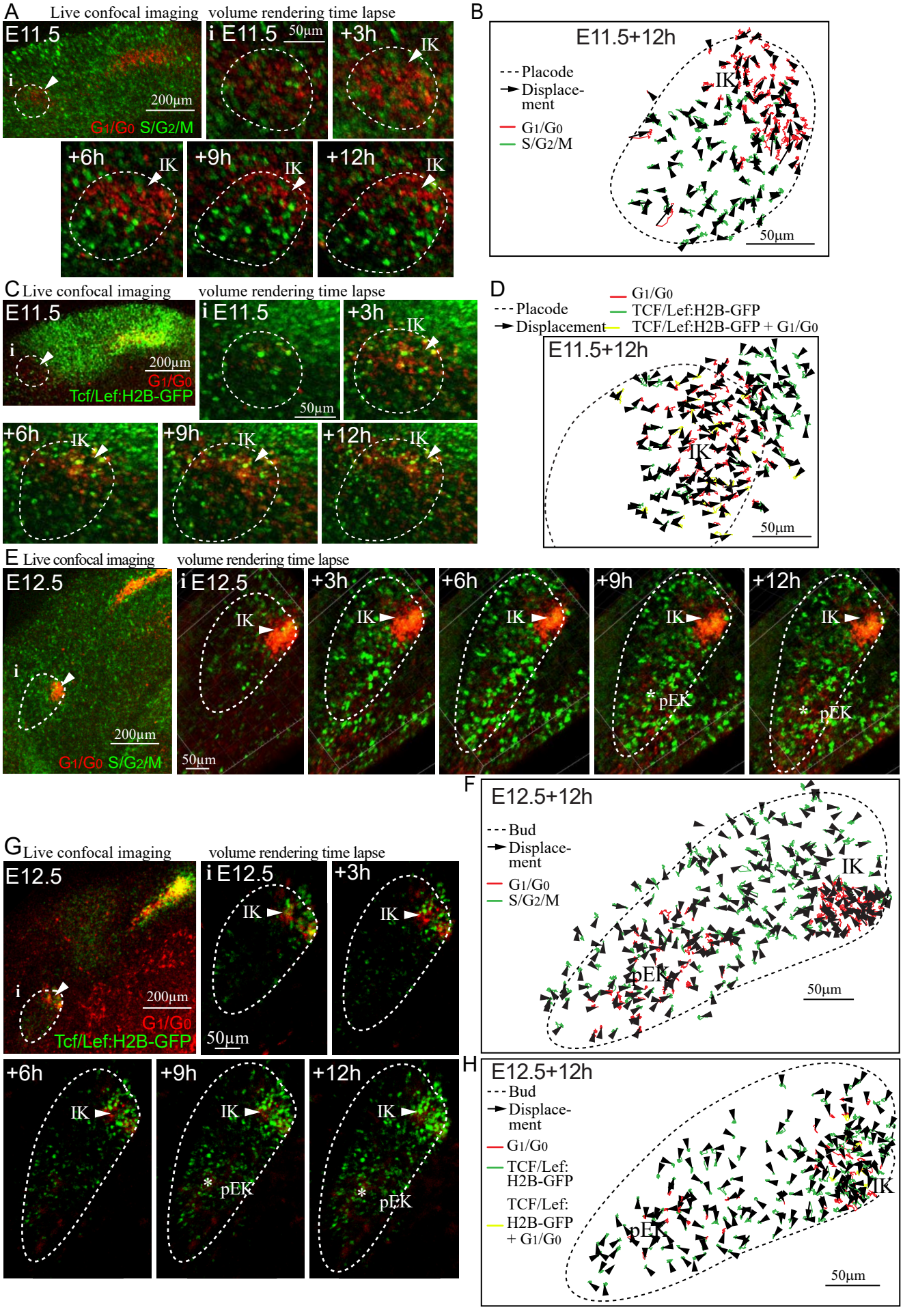
A
Live confocal imaging
volume rendering time lapse
E11.5
i
200μm
G1/G0 S/G2/M
i E11.5
50μm
+3h
IK
+6h
IK
+9h
IK
+12h
IK
B
E11.5+12h
Placode
Displace-
ment
G1/G0
S/G2/M
IK
50μm
C
Live confocal imaging
volume rendering time lapse
E11.5
i
200μm
G1/G0
Tcf/Lef:H2B-GFP
i E11.5
50μm
+3h
IK
+6h
IK
+9h
IK
+12h
IK
D
Placode
Displacement
G1/G0
TCF/Lef:H2B-GFP
TCF/Lef:H2B-GFP + G1/G0
E11.5+12h
IK
50μm
E
Live confocal imaging
volume rendering time lapse
E12.5
i
200μm
G1/G0 S/G2/M
i E12.5
50μm
+3h
IK
+6h
IK
+9h
IK
*
pEK
+12h
IK
*
pEK
F
E12.5+12h
Bud
Displace-
ment
G1/G0
S/G2/M
IK
pEK
50μm
G
Live confocal imaging
volume rendering time lapse
E12.5
i
200μm
G1/G0
Tcf/Lef:H2B-GFP
i E12.5
50μm
+3h
IK
+6h
IK
+9h
IK
*
pEK
+12h
IK
*
pEK
H
E12.5+12h
Bud
Displace-
ment
G1/G0
TCF/Lef:
H2B-GFP
TCF/Lef:
H2B-GFP
+ G1/G0
IK
pEK
50μm

Figure 5.

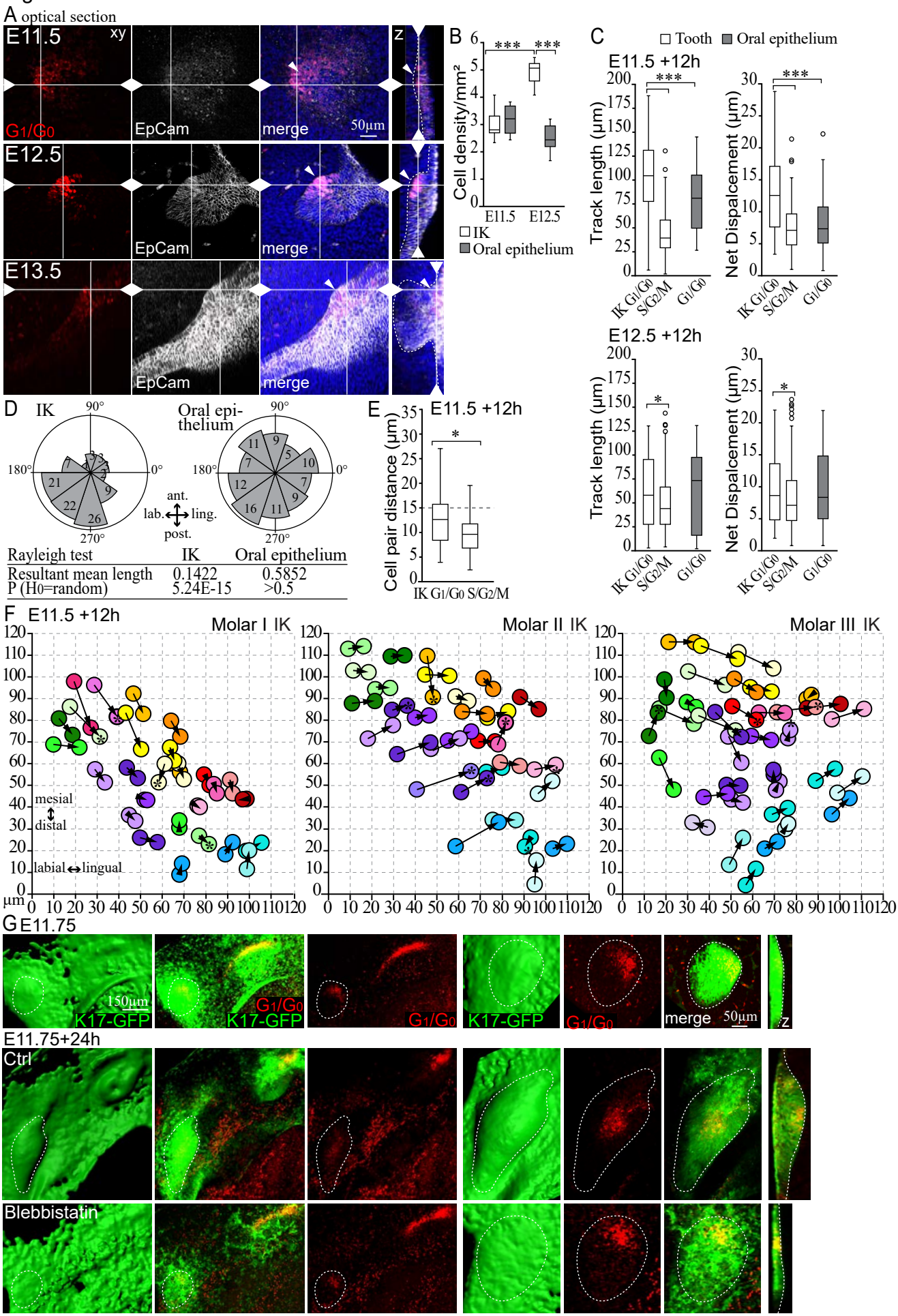
A optical section
E11.5
xy
z
G1/G0
EpCam
merge
50µm
E12.5
E13.5
B
Cell density/mm²
E11.5
E12.5
IK
Oral epithelium
C
Tooth
Oral epithelium
E11.5 +12h
Track length (µm)
Net Dispalcement (µm)
IK G1/G0
S/G2/M
G1/G0
E12.5 +12h
D
IK
Oral epi-thelium
ant.
lab.
ling.
post.
Rayleigh test
Resultant mean length
P (H0=random)
0.1422
5.24E-15
0.5852
>0.5
E
E11.5 +12h
Cell pair distance (µm)
IK G1/G0 S/G2/M
F
E11.5 +12h
Molar I IK
Molar II IK
Molar III IK
mesial
distal
labial↔lingual
µm
G
E11.75
150µm
K17-GFP
G1/G0
merge
50µm
z
E11.75+24h
Ctrl
Blebbistatin

Figure 6.

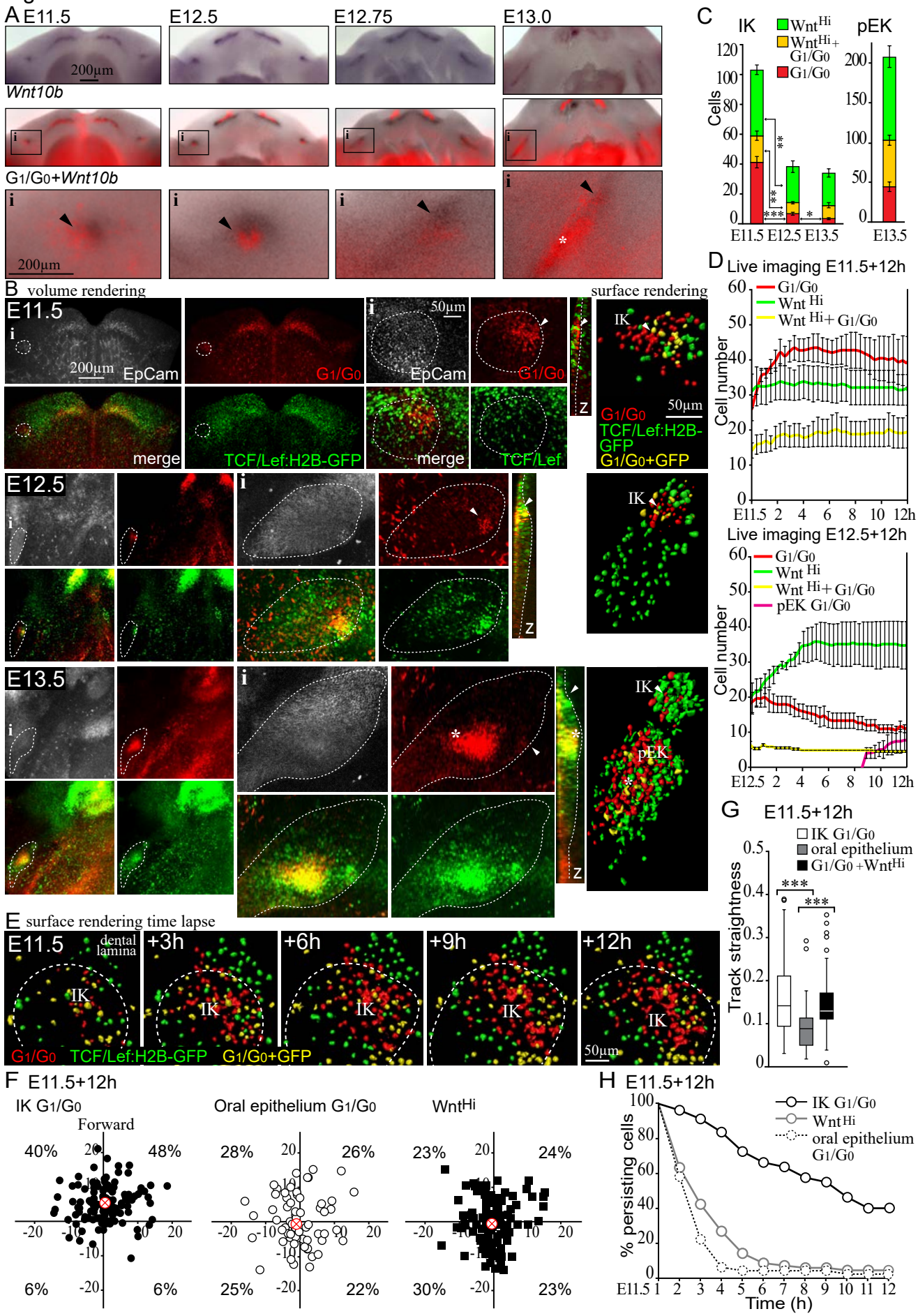
A E11.5
E12.5
E12.75
E13.0
200μm
Wnt10b
G1/G0+Wnt10b
B volume rendering
surface rendering
E11.5
EpCam
G1/G0
merge
TCF/Lef:H2B-GFP
TCF/Lef
50μm
IK
G1/G0+GFP
E12.5
E13.5
pEK
C
IK
pEK
Wnt Hi
Wnt Hi+ G1/G0
G1/G0
Cells
E11.5 E12.5 E13.5
E13.5
D Live imaging E11.5+12h
Wnt Hi
Wnt Hi+ G1/G0
Cell number
E11.5 2 4 6 8 10 12h
Live imaging E12.5+12h
pEK G1/G0
E12.5 2 4 6 8 10 12h
G E11.5+12h
IK G1/G0
oral epithelium
G1/G0 +Wnt Hi
Track straightness
***
E surface rendering time lapse
dental lamina
+3h
+6h
+9h
+12h
F E11.5+12h
IK G1/G0
Forward
40%
48%
6%
Oral epithelium G1/G0
28%
26%
25%
22%
Wnt Hi
23%
24%
30%
23%
H E11.5+12h
IK G1/G0
Wnt Hi
oral epithelium G1/G0
% persisting cells
Time (h)

Figure 7.

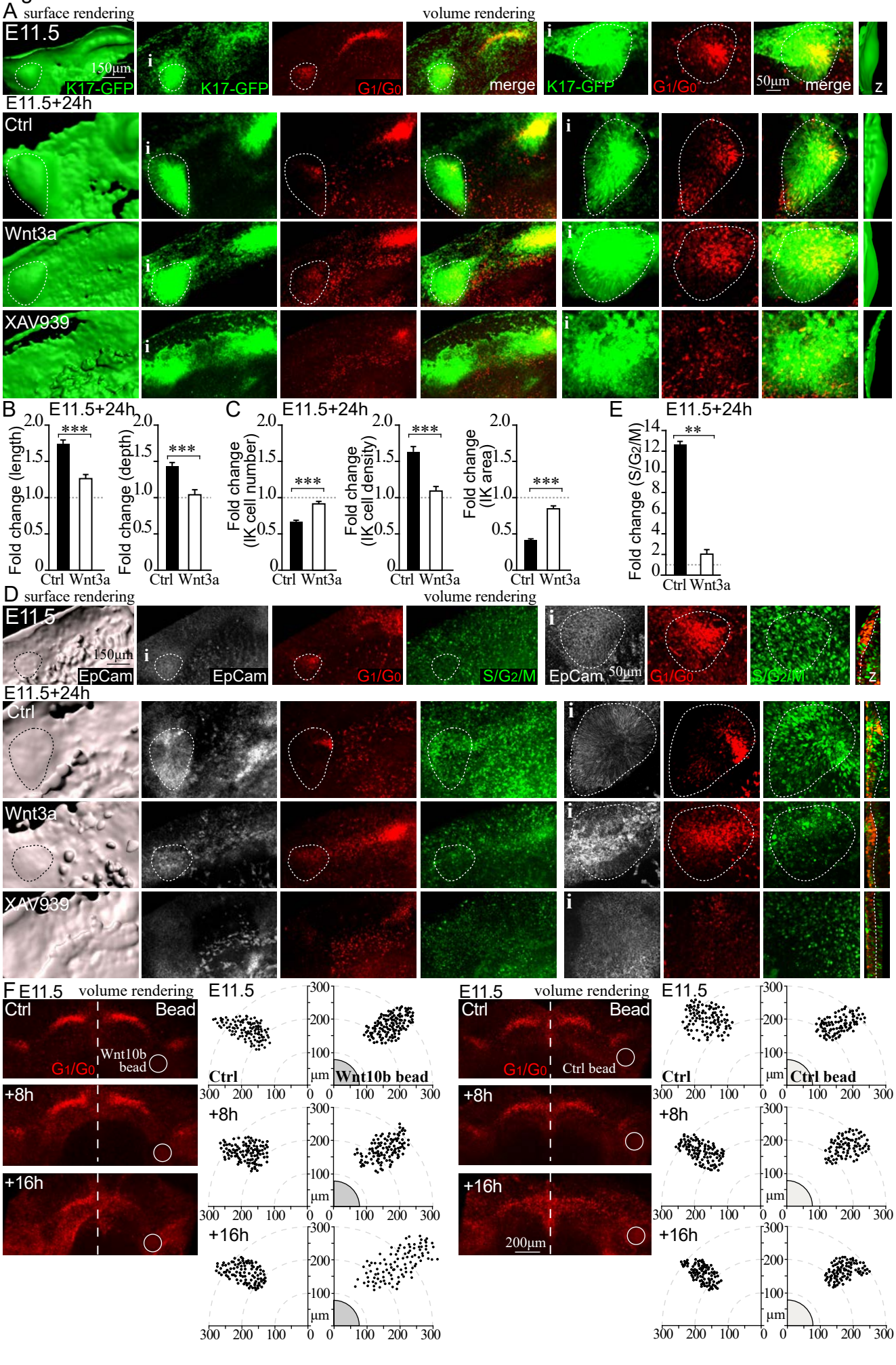
A surface rendering
volume rendering
E11.5
150μm
K17-GFP
i
K17-GFP
G1/G0
merge
i
K17-GFP
G1/G0
50μm
merge
z
E11.5+24h
Ctrl
Wnt3a
XAV939
B
E11.5+24h
Fold change (length)
Fold change (depth)
***
Ctrl Wnt3a
C
E11.5+24h
Fold change (IK cell number)
Fold change (IK cell density)
Fold change (IK area)
***
Ctrl Wnt3a
E
E11.5+24h
Fold change (S/G2/M)
**
Ctrl Wnt3a
D surface rendering
volume rendering
E11.5
150μm
EpCam
i
EpCam
G1/G0
S/G2/M
i
EpCam
50μm
G1/G0
S/G2/M
z
E11.5+24h
Ctrl
Wnt3a
XAV939
F E11.5 volume rendering
Ctrl
Bead
G1/G0
Wnt10b bead
+8h
+16h
E11.5
Ctrl
Wnt10b bead
+8h
+16h
E11.5 volume rendering
Ctrl
Bead
G1/G0
Ctrl bead
+8h
+16h
200μm
E11.5
Ctrl
Ctrl bead
+8h
+16h
μm

Supplemental Figure S1. (related to Figure 1)

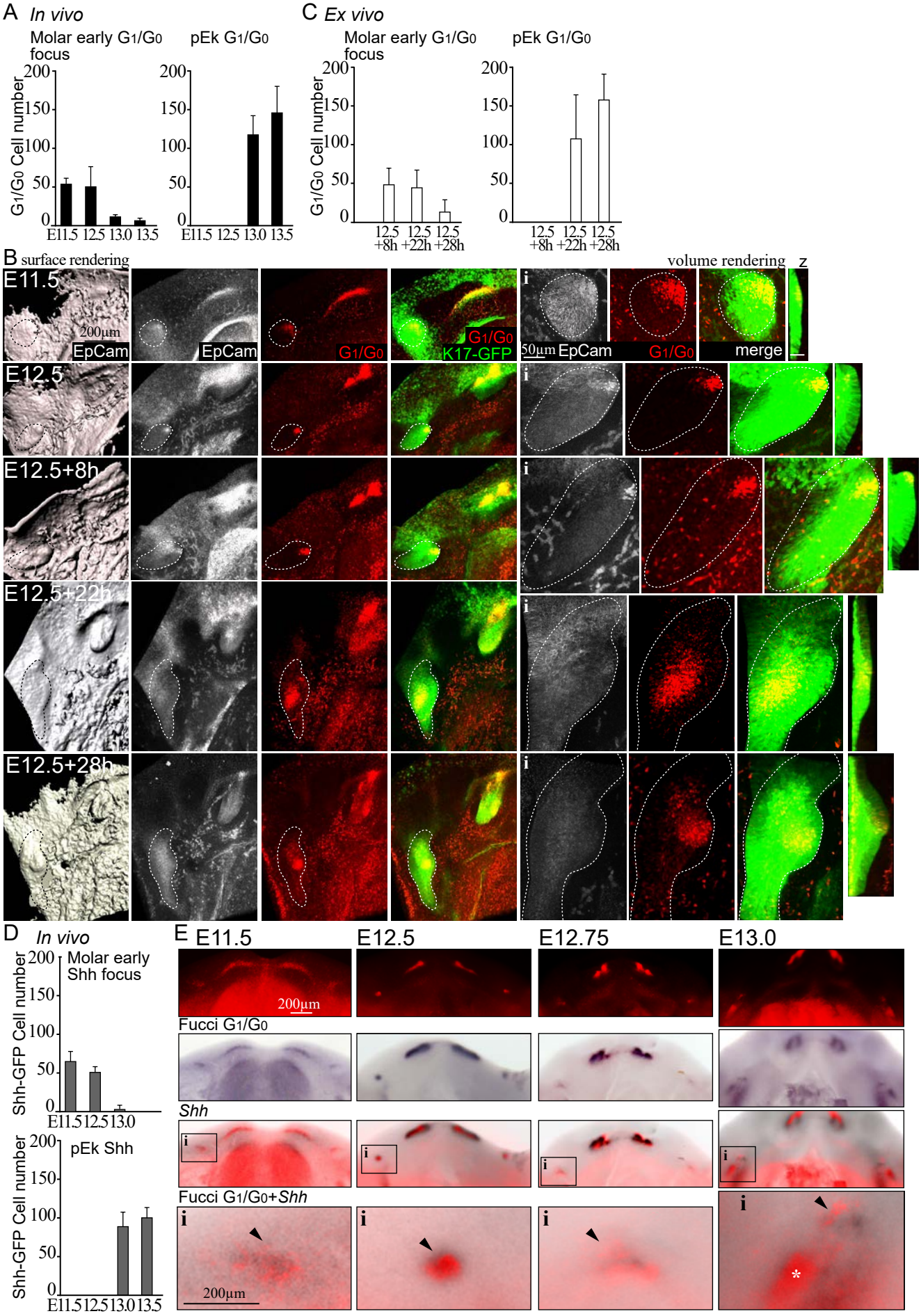

Supplemental Figure S2. (related to Figure 2.)

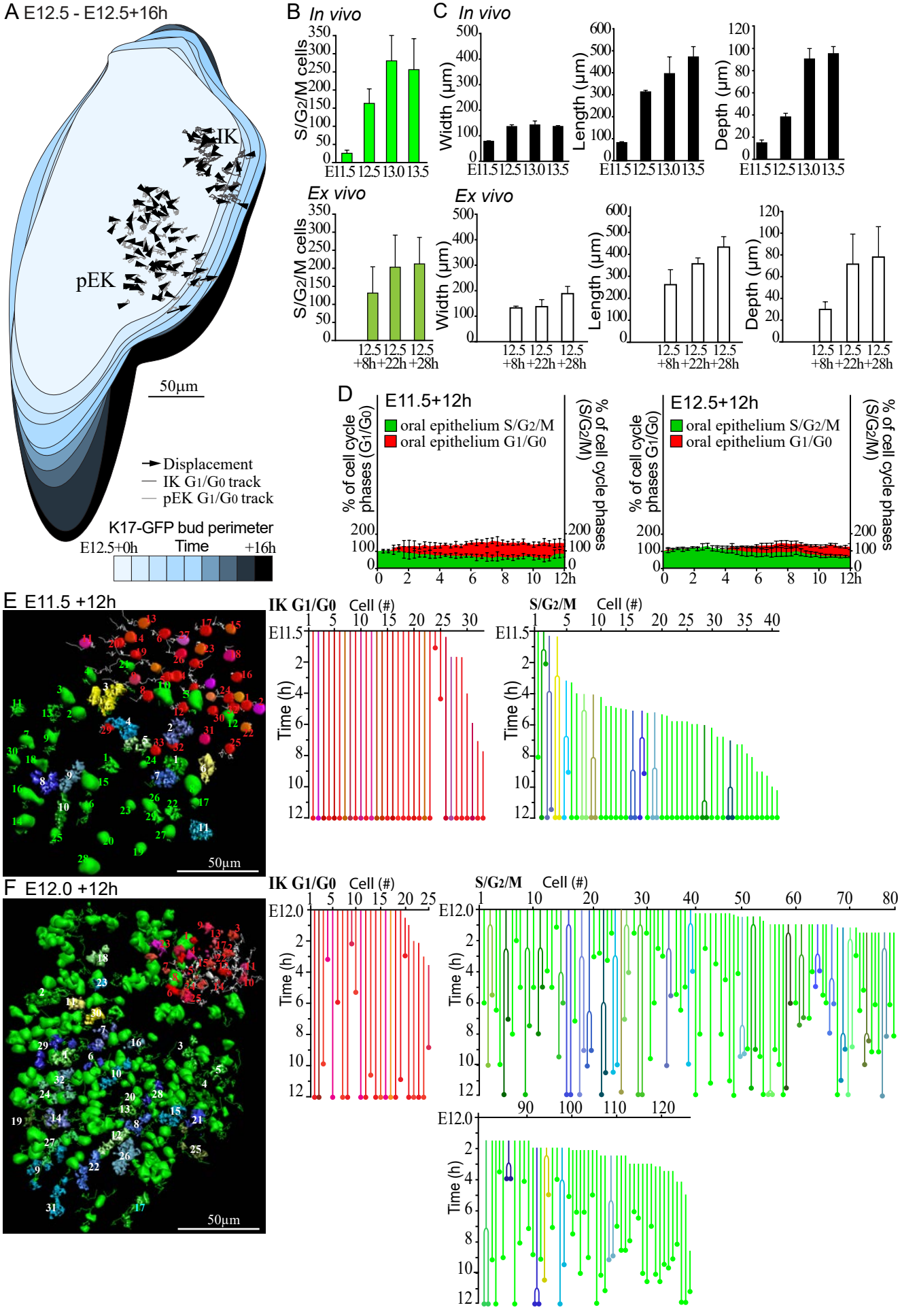

Supplemental Figure S3. (related to Figure 2.)

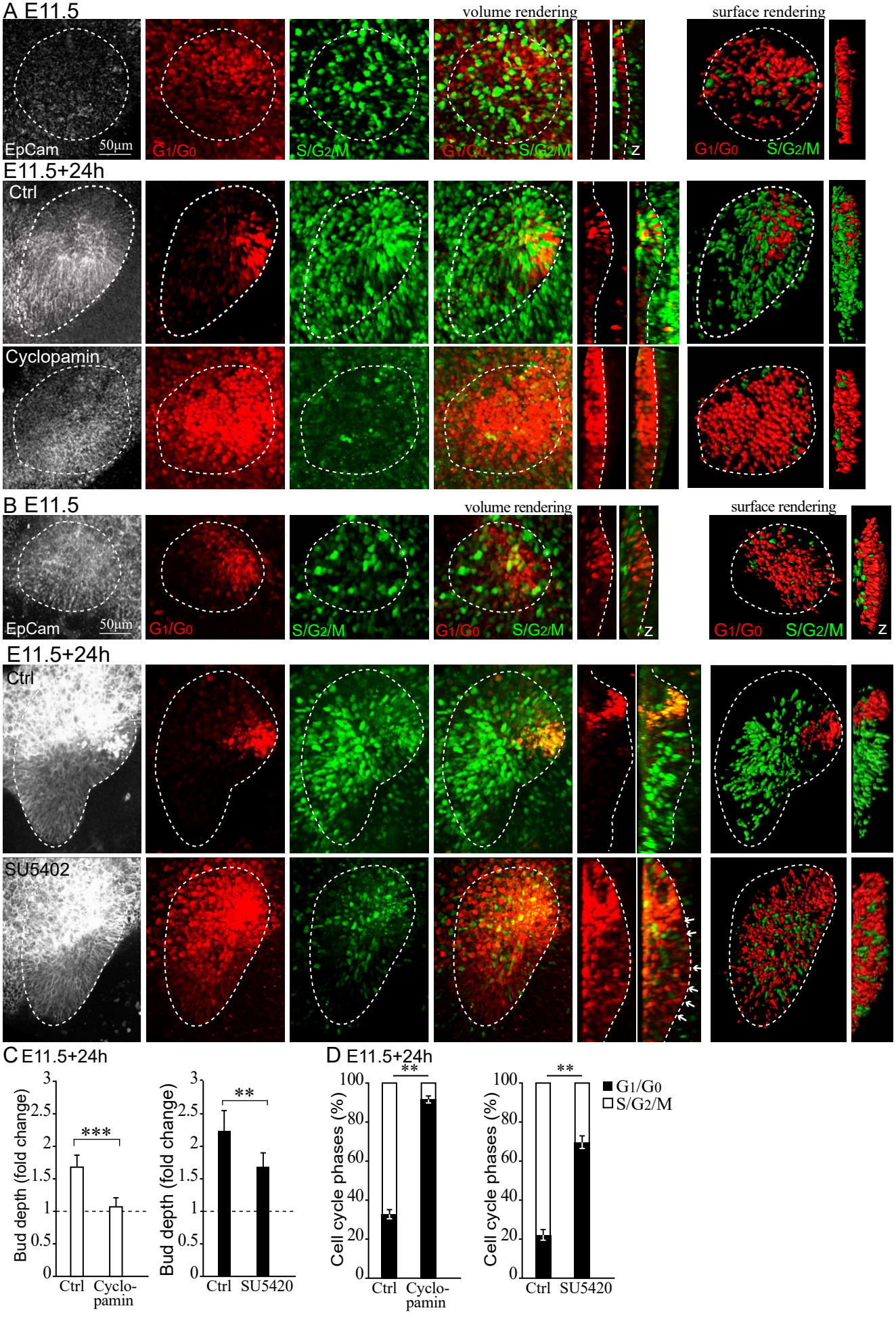

Supplemental Figure S4. (related to Figure 3.)

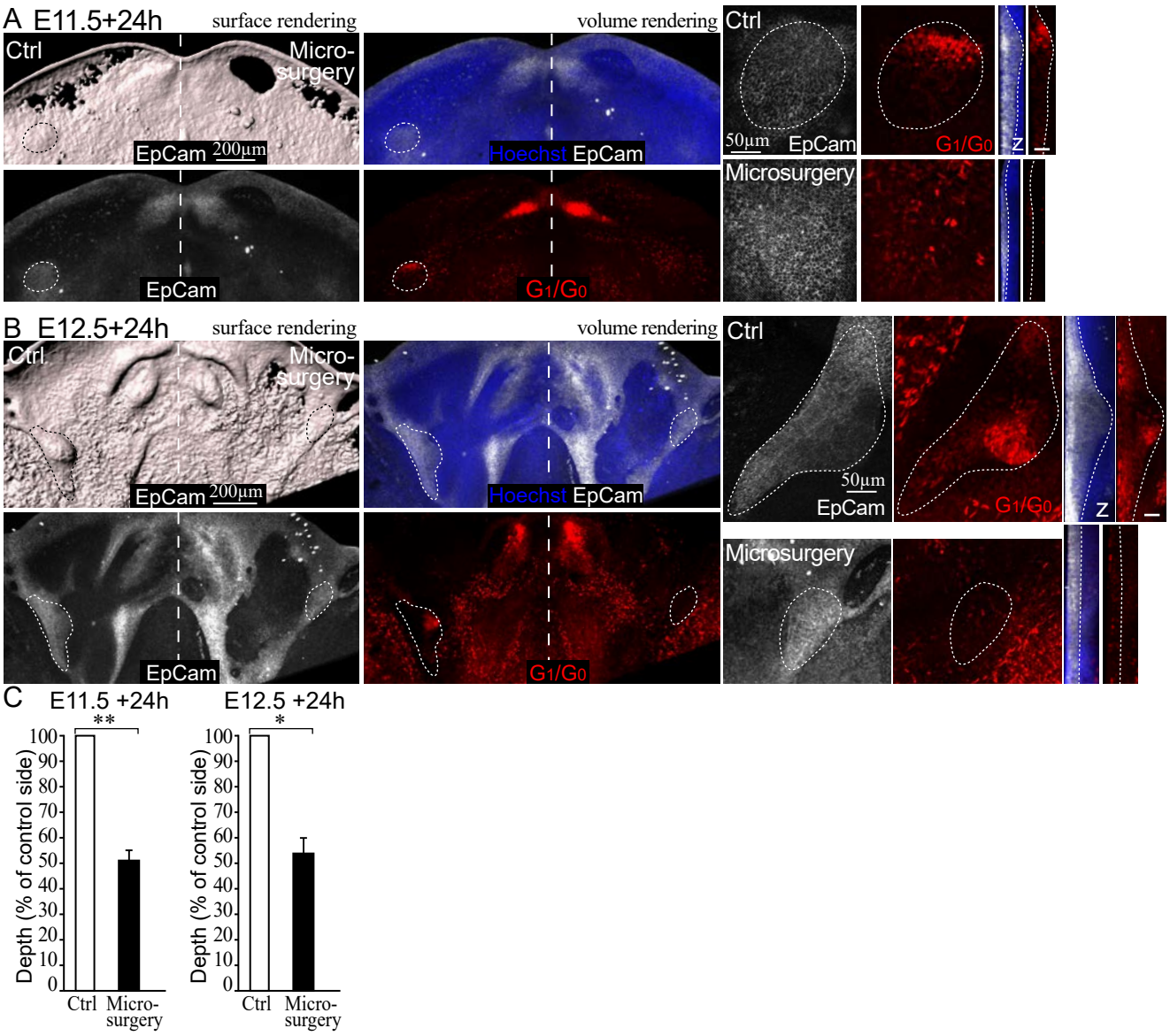

Supplementary Figure S5. (related to Figure 6.)

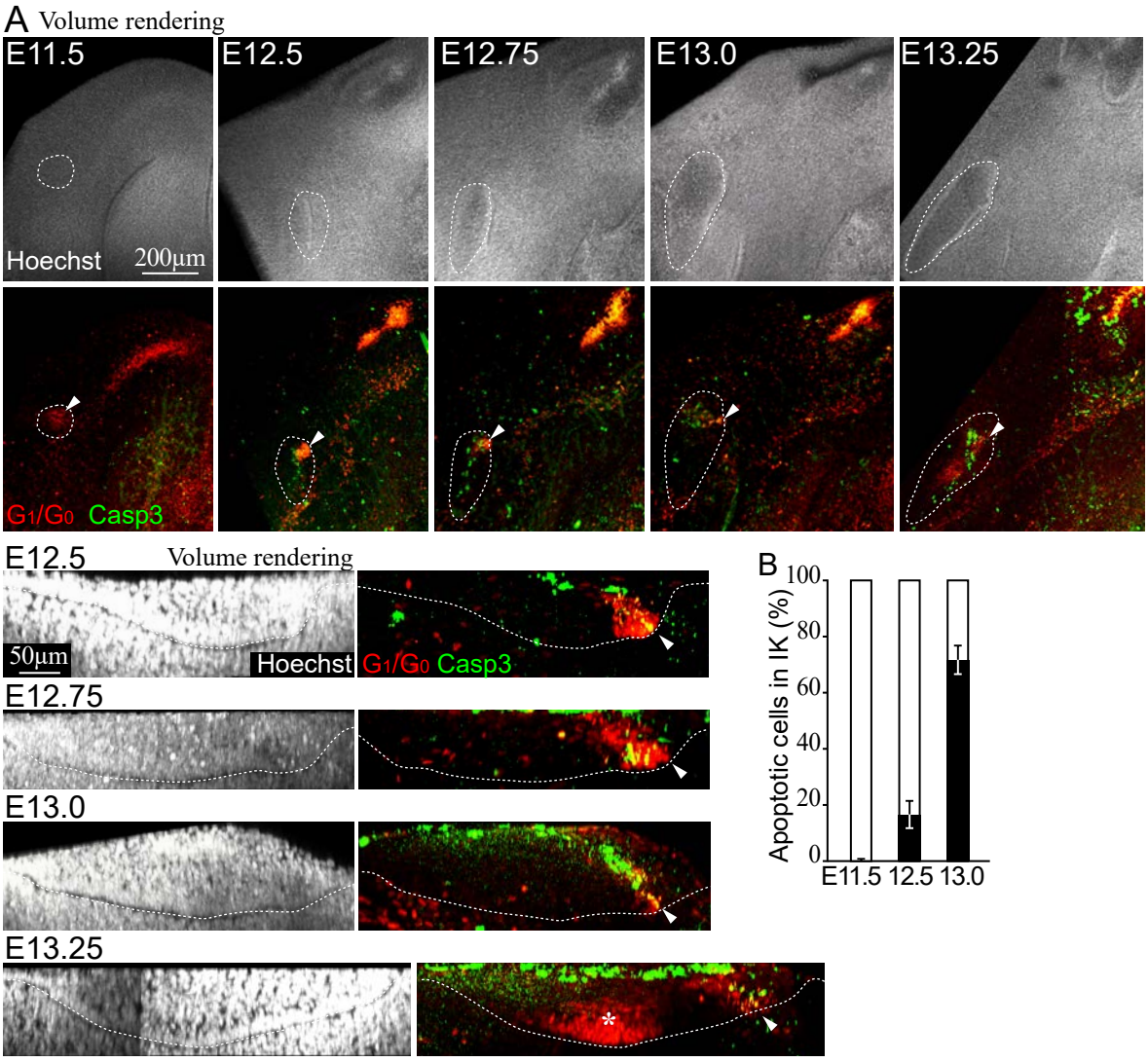

Supplemental Figure S6. (related to Figure 7.)